

Quasi-Stellar Objects, Ultraluminous IR Galaxies, and Mergers¹

Gabriela Canalizo²

Institute for Astronomy, University of Hawaii, and the Institute of Geophysics and Planetary Sciences, Lawrence Livermore National Laboratory, 7000 East Avenue, L413, Livermore, CA 94550

Alan Stockton²

Institute for Astronomy, University of Hawaii, 2680 Woodlawn Drive, Honolulu, HI 96822

ABSTRACT

We test the hypothesis that QSOs are formed via strong tidal interactions or mergers, initially going through an ultraluminous infrared phase. Our approach is to look for traces to this phase in the host galaxies of QSOs. We select a sample of low-redshift bona fide QSOs that may be in a transitional stage between ULIGs and QSOs. These objects, which we shall call transition QSOs, have an intermediate position in the far infrared color-color diagram between the regions occupied by the two classes of objects. We carry out a systematic spectroscopic and imaging study of these objects in order to determine their interaction and star-forming histories. By modeling the spectra, we obtain ages for the recent starburst events in the host galaxies and interacting companions. We have discussed in detail the first 5 objects in the sample in previous publications; here we present results for the remaining 4 objects, and discuss the sample as a whole. We find that all 9 transition QSOs are undergoing tidal interactions and that 8 are major mergers. Every object also shows strong recent star-forming activity, and in at least eight cases this activity is directly related to the tidal interaction. The ages we derive for the starburst populations range from currently active star formation in some objects, to post-starburst ages $\lesssim 300$ Myr in others. There is also a clear connection between interactions, starbursts, and QSO activity. Seven of the QSOs in the sample are also ULIGs; statistical considerations show

¹Based on observations with the NASA/ESA Hubble Space Telescope, obtained from the data archive at the Space Telescope Science Institute, which is operated by the Association of Universities for Research in Astronomy, Inc. under NASA contract No. NAS5-26555.

²Visiting Astronomer, W.M. Keck Observatory, jointly operated by the California Institute of Technology and the University of California.

that the two phenomena are necessarily physically related in these objects. Our results imply one of two scenarios: (1) at least some ULIGs evolve to become classical QSOs, and the transition stage lasts $\lesssim 300$ Myr, or (2) at least some QSOs are born under the same conditions as ULIGs, and their lifetime as QSOs lasts $\lesssim 300$ Myr. We discuss other properties and trends found in the sample, and propose a model that accounts for all of them, as well as the youth of these systems.

Subject headings: galaxies: interactions — galaxies: infrared — galaxies: starburst — galaxies: evolution — quasars: individual (IRAS 00275–2859, IRAS 04505–2958, PG 1543+489, and I Zw 1)

1. Introduction

It is now widely accepted that the energy source powering QSOs is gravitational in nature and that it involves some form of accretion of matter onto a compact massive object in the center of a galaxy, as first suggested by Lynden-Bell (1969). But it has long been clear that such an object will fairly quickly swallow up most of the material that comes within its vicinity and normal relaxation processes repopulate such orbits far too slowly to sustain the power output of a QSO. We are left with the problem first clearly posed by Gunn (1979): how does one feed the monster? As if anticipating the problem, Toomre & Toomre (1972) suggested the importance of interactions and mergers as fueling mechanisms in the section “Stoking the Furnace?” of their classic paper “Galactic Bridges and Tails”, where they muse: “Would not the violent mechanical agitation of a close tidal encounter—let alone an actual merger—already tend to bring *deep* into a galaxy a fairly *sudden* supply of fresh fuel in the form of interstellar material, either from its own outlying disk or by accretion from its partner?” Toomre & Toomre’s suggestion was specifically in reference to galaxies showing vigorous nuclear star formation. However, it was only a small step to apply the same scenario to QSO activity, a connection explicitly made by Stockton (1982) in a study of compact companions to QSOs.

Many attempts to connect most or all QSO activity with interactions and mergers followed, and circumstantial evidence supporting this connection was rapidly accumulated. A variety of morphological distortions were seen in the host galaxies, ranging from simple asymmetries to clear bridge-like or tail-like structures (*e.g.*, Gehren et al. 1984; Hutchings et al. 1984; Hutchings, Johnson, & Pyke 1988; Stockton & MacKenty 1987). There seemed to be a statistical excess of close companion galaxies (*e.g.*, Heckman et al. 1984). Highly structured distributions of extended ionized gas were found around QSOs (*e.g.*, Boroson,

Persson, & Oke 1985; Stockton & MacKenty 1987). Stockton (1990) reviews and evaluates these and other examples and points out that what keeps these observations from having more weight as evidence for a connection between interactions and the triggering of QSO activity is the lack of a suitable control sample.

It was in this context that the *Infrared Astronomical Satellite (IRAS)* made the remarkable discovery of a new class of galaxies, the luminous infrared galaxies, which emit the bulk of their energy at infrared wavelengths (Houck et al. 1984; Soifer et al. 1984a,b). Many of these galaxies showed unambiguous signs of tidal interaction (Allen, Roche, & Norris 1985; Sanders et al. 1986; Armus, Heckman, & Miley 1987), and the interaction rate was observed to increase with luminosity. In particular, virtually all of the ultraluminous infrared galaxies (*i.e.*, those having luminosities $> 10^{12} L_{\odot}$; henceforth ULIGs), were found to be involved in mergers (see Sanders & Mirabel 1996 for a review).

Up until the time of *IRAS*, QSOs were the only objects known to have bolometric luminosities greater than $10^{12} L_{\odot}$, so it was natural to speculate about about a relation between QSOs and the newly discovered ULIGs. Sanders et al. (1988) noticed that ULIGs and QSOs had not only similar bolometric luminosities, but also similar space densities. In other words, ULIGs were numerous enough to be the parent population for QSOs, and their infrared luminosities could simply be due to QSO flux being re-radiated at longer wavelengths. This led Sanders et al. (1988) to suggest that ULIGs may play a dominant role in the formation of all QSOs. The picture put forward was that ULIGs were the result of strong interactions or mergers which funneled gaseous material into the central regions of galaxies, thus fueling intense star formation and the QSO activity. ULIGs were then dust-enshrouded QSOs which, after blowing away the dust, became classical QSOs.

This hypothesis has sparked much debate regarding the main source that powers ULIGs: is it powerful starbursts (Joseph 1999) or AGNs (Sanders 1999)? Smith, Lonsdale, & Lonsdale (1998; see also Lonsdale, Smith, & Lonsdale 1993, 1995) have looked for the presence or absence of a true high brightness temperature AGN-like radio core in ULIGs; Genzel et al. (1998) and Lutz et al. (1998) use the strength of the $7.7 \mu\text{m}$ PAH line to continuum ratio to determine the fraction of the infrared/submillimeter luminosity peak in spectral energy distributions (SEDs) that is due to a starburst and an AGN respectively, and Lutz, Veilleux, & Genzel (1999) have compared the dominant contributor from this analysis with the classification from optical/IR emission lines, finding general agreement; Nakagawa et al. (1999) have used *ASCA* hard x-ray observations to estimate the AGN contribution to the total luminosity; Hines et al. (1995, 1999a), Goodrich et al. (1996) and Tran et al. (1999), among others, have looked for hidden QSO broad emission lines in scattered polarized light in ULIGs. These are only a few examples of the myriad of tests at virtually every observable

wavelength that have been applied to ULIGs with the goal of determining the nature of the main energy source. Although some uncertainty remains, it appears that $\sim 30\%$ of ULIGs are dominated by AGNs (Lutz, Veilleux, & Genzel 1999) and that this fraction rises at the highest luminosities (Veilleux 1999).

The limited attempts to address the question of evolution from the other side of the fence (in other words, to look at QSO host galaxies specifically in search for traces of a ULIG phase) pale in comparison. Progress in this area has been damped by the difficulty in studying QSO host galaxies, as observations are invariably hampered by the enormous brightness of the QSO nuclei. It is not too surprising that even *Hubble Space Telescope* (*HST*) observations of host galaxies caused some confusion at first. Bahcall, Kirhakos, & Schneider (1995) originally presented a scandalous set of “naked” QSOs, claiming that no galaxy as bright as L^* could be detected in 5 out of a sample of 8 low-redshift QSOs. Later, McLeod & Rieke (1995) showed that, with suitable smoothing, L^* galaxies were indeed detectable on the same *HST* images, and concluded that most QSOs are in normal, early-type galaxies. Efforts in the last decade have concentrated on characterizing QSO host galaxies and, in particular, searching for any possible differences between the hosts of radio-loud and radio-quiet objects (*e.g.*, McLure et al. 1999; Bahcall et al. 1997; Boyce et al. 1998), as well as continuing to explore the connection to interactions and mergers as means to trigger the nuclear activity (*e.g.*, Hutchings et al. 1994; McLeod & Rieke 1994; Disney et al. 1995; Hutchings & Neff 1992; Bahcall et al. 1997; Boyce et al. 1996). Nevertheless, all the evidence connecting QSOs to mergers remains *circumstantial*.

Systematic studies to attempt to trace QSOs to ULIGs have been few and limited to imaging studies of host galaxy morphologies. Surace (1998) observed a complete sample of PG QSOs with infrared excesses similar to those of warm ULIGs. He finds that 22% are unmistakably the result of galaxy mergers, and that the *H*-band luminosities of the hosts of all the objects in the sample are consistent with those found in ULIGs. Clements (2000) compares the far infrared properties of QSOs in disturbed and undisturbed hosts in the PG survey, and finds that the mean 60 μm luminosity of the QSOs with disturbed hosts is several times greater than that of QSOs with undisturbed hosts. This result would be in agreement with a scenario where the disturbed-host QSOs are at an earlier stage in their evolution from ULIGs to classical QSOs.

These and other efforts have concentrated on the connection between QSOs and ULIGs via morphologies indicative of mergers. An area that has been virtually ignored, except for the occasional qualitative comment, is the detailed study of the potential connection between both families via *starbursts*. While the starburst–AGN connection itself has been the subject of much recent research, no systematic effort has been made to attempt to detect

such starbursts in the host galaxies of QSOs. In particular, relatively few spectroscopic observations of QSO host galaxies have been published (Boroson & Oke 1982, 1984; Boroson, Oke, & Green 1982; Balick & Heckman 1983; Mackenty & Stockton 1984; Boroson, Persson, & Oke 1985; Hickson & Hutchings 1987; Hutchings & Crampton 1990). The majority of these have been limited to reporting the presence of absorption lines in the spectra of host galaxies, and most studies have been of isolated cases. Again, this is not surprising considering the difficulties in observing a low surface brightness object only a few arcseconds (in the best of cases) away from its ~ 1000 times brighter nucleus. One group (Hughes et al. 2000; Nolan et al. 2000) is currently carrying out a systematic spectroscopic study of radio galaxies and both radio-loud and radio-quiet QSOs, but their emphasis is in characterizing the old populations (while treating any possible recent starburst components as a nuisance) and describing differences among the hosts of the three classes of objects. Thus, it is in this mostly unexplored territory of spectroscopy of QSO host galaxies that we have focussed our efforts.

Our approach to the question of evolution is as follows: in the evolutionary scenario, objects are expected to transition at some point from an ultraluminous infrared phase to a “normal” QSO phase; we shall refer to objects in this latter phase as “classical QSOs.” Our intent is to define a group of “transition” objects, *i.e.*, objects that share characteristics with both QSOs and ULIGs, and, through both imaging and spectroscopic observations, answer the questions: “*Where did they come from?*”, and “*Where will they go?*” If the answers to these questions were unambiguously determined to be, respectively, “from the ULIG population,” and “to the classical QSO population”, the evolutionary scenario would be confirmed for at least one class of QSOs, and statistical considerations could then tell us whether the process is relevant to the majority of QSOs. In the following section we address the problem of how to come up with a sample of transition objects, describe our selection criteria, and present our sample. Results for the first 5 objects in the sample have been published in Canalizo & Stockton (1997), Canalizo & Stockton (2000a), Canalizo & Stockton (2000b), and Stockton, Canalizo, & Close (1998) (hereafter CS97, CS00a, CS00b, and SCC98, respectively). In §3 we analyze and present results for the last 4 objects in the sample: IRAS 00275–2859, IRAS 04505–2958, PG 1543+489, and IZw 1. In §4 we summarize the observed and derived properties of all the objects in the sample, in §5 we discuss these properties individually, and in §6 we present a model that accounts for all of them in the context of our main results. We discuss other possible tests of the evolutionary paradigm in §7 and present an overview and summary in §8.

2. Sample Selection

It is possible to select a sample of objects that may be in some transitional phase by choosing a set of bona fide QSOs that share a given characteristic with ULIGs. We could, for example, choose those QSOs that have recent signs of interaction. However, the selection of such a sample would be very subjective, and it would be virtually impossible to collect a complete sample and/or to come up with a suitable control sample. In an effort to avoid some of these problems, we have chosen to use far infrared colors to form a nearly complete sample.

The far infrared (FIR) color-color diagram has been used as a tool to detect and discriminate between different types of activity in the nuclear and circumnuclear regions of galaxies. The spectral indices plotted in the diagram are $\alpha(100, 60)$ and $\alpha(60, 25)$, which are obtained from the *IRAS* flux densities at 100 μm , 60 μm , and 25 μm . Different kinds of objects, such as QSOs/Seyferts, starbursts, and powerful IR galaxies, occupy fairly well defined regions in the diagram (see, *e.g.*, Neugebauer, Soifer, & Miley 1985; de Grijp, Miley, & Lub 1987; Taniguchi et al. 1988; L ipari 1994). Objects whose FIR fluxes are dominated by reradiation from dust will be preferentially located around the black-body region of the diagram, while those with strong non-thermal emission, such as optically selected QSOs, are found near the power-law region (see Fig. 1).

Neugebauer, Soifer, & Miley (1985) plot in the FIR diagram the 22 QSOs detected in the *IRAS* all-sky survey which have good quality fluxes at the relevant bands (see their Fig. 1), and note that the majority (19) lie close to the line of constant spectral index (dubbed Power-Law in Fig. 1). Stockton & Ridgway (1991) noticed that the other three QSOs, which fell near the region of the diagram occupied by luminous IR galaxies (Mrk 231, Mrk 1014, and 3C 48) were also at the time the three QSOs that were arguably the three best examples of QSOs that showed apparent stellar tidal tails. Stockton & Ridgway proposed that these QSOs are either transitional objects in an evolutionary scenario, or exceptional or extreme examples which are distinct from the general QSO population.

L ipari (1994) found an independent correlation using the FIR diagram: infrared-loud AGN having extreme Fe II emission have positions intermediate between the black-body and power-law regions, while those having less extreme, but still strong, Fe II emission lie closer to the power-law region. L ipari proposed that the strength of the Fe II emission lines might be associated with the phase of the starburst/superwind of Type II supernovae (Terlevich et al. 1992). Extreme Fe II emitters would then be ULIGs at the end phase of a strong starburst, and strong emitters would be post-starburst objects.

The FIR diagram provides us with an opportunity to select a complete sample from

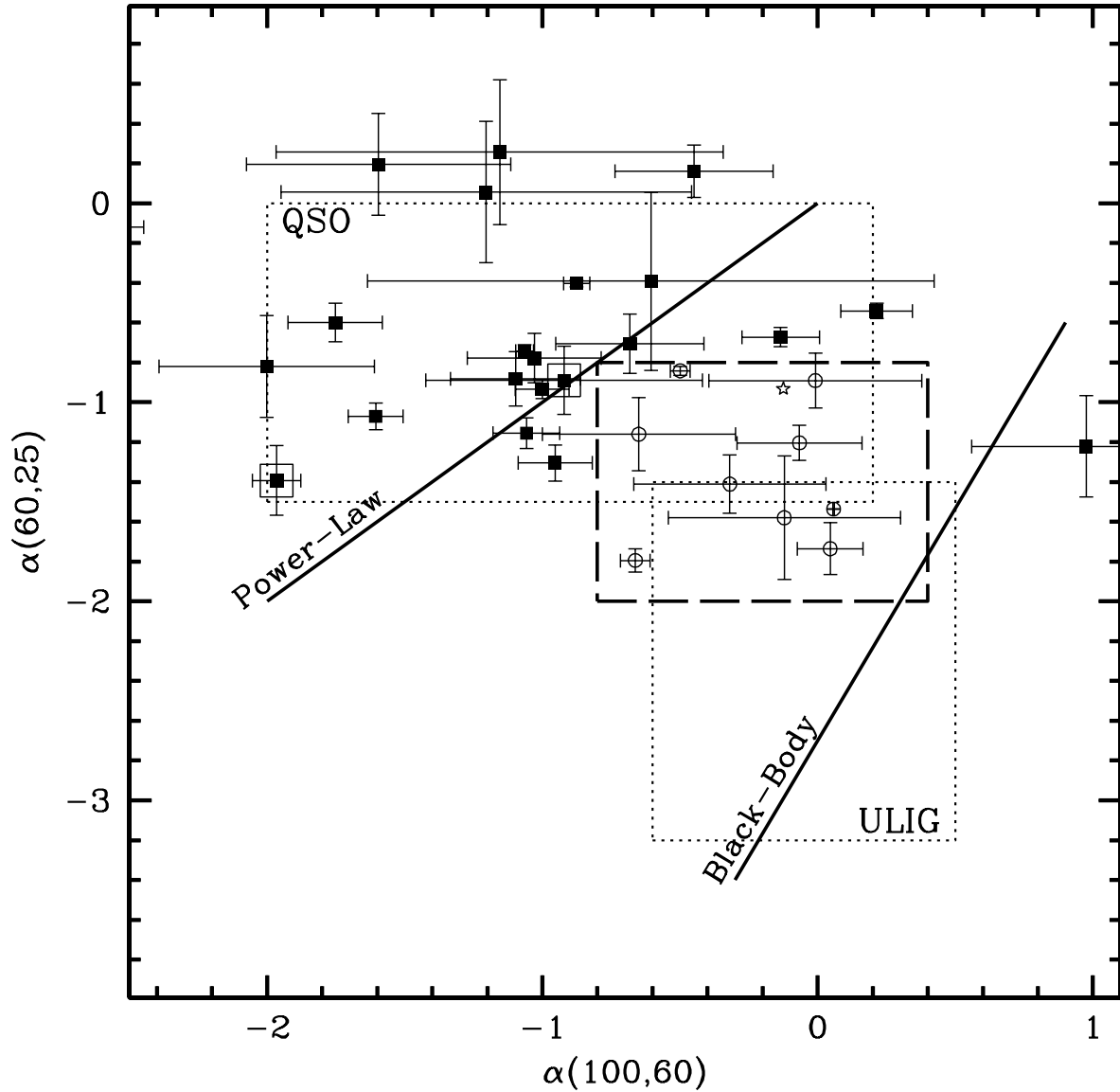


Fig. 1.— Far infrared color-color diagram (adapted from L ipari 1994). Every object from the three samples described in the text that satisfies selection criteria 1 through 4 is plotted in this diagram. The color limits for our sample of transition QSOs are indicated by the long dashed lines. Objects in our sample are plotted as open circles while all others are plotted as filled squares. The two filled squares surrounded by large open squares are PHL 909 (left) and IRAS 14026+4341 (right); these objects are discussed in §7.3 and §5.5, respectively. The star indicates the position of Mrk 509. The QSO and ULIG loci, both empirically determined, are indicated by the dotted rectangles.

those objects which have firm detections in the three relevant IRAS bands. The precise color limits we choose (see below) are somewhat arbitrary and are simply meant to define a reasonable sample of objects spanning a region in the FIR two-color diagram intermediate between the ULIG and classical QSO populations.

2.1. Selection Criteria

Our goal is to collect as complete a sample as possible of low-redshift, bona-fide QSOs with an intermediate position in the FIR color–color diagram. Our selection criteria are:

1. a luminosity above the cutoff defined for quasars by Schmidt & Green (1983), *i.e.*, $M_B = -21.5 + 5 \log h$ (or $M_B = -22.1$ for $H_0 = 75 \text{ km s}^{-1} \text{ Mpc}^{-1}$),
2. a redshift $z \leq 0.4$,
3. a declination $\delta \geq -30^\circ$,
4. firm *IRAS* detections at $25 \mu\text{m}$, $60 \mu\text{m}$, and $100 \mu\text{m}$, and
5. a position in the FIR color–color diagram which is intermediate between the ULIG and QSO loci, *i.e.*, in the region delimited by $-0.8 < \alpha(100, 60) < 0.4$ and $-2.0 < \alpha(60, 25) < -0.8$

Our starting point was the sample of 179 QSOs observed with *IRAS* published by Neugebauer et al. (1986). To this sample we added the sample of warm objects by Low et al. (1988), where they find 6 previously unidentified QSOs from a list of 187 sources. Finally, we added the sample of 91 ULIGs (of which 65 were newly discovered) by Clements et al. (1996a), since some of these objects have AGNs which could possibly have QSO luminosities. Since none of these samples is complete, our sample cannot be complete. However, to the best of our knowledge, we have included *every known bona-fide QSO* which satisfies the 5 selection criteria.

There are a few objects that will be either within or outside the sample color limits depending on which published *IRAS* flux values are used. We give priority to the flux values given by Neugebauer et al. (1986), since the majority of the QSOs in that sample have “pointed observations” in addition to the all-sky survey observations. The additional observations result in an increase in sensitivity by a factor of ~ 5 . Evidently, no pointed observations are available for those objects which were discovered by *IRAS* itself; we use flux values from the Faint Source Catalog for these.

The restriction that objects in the sample must have firm detections at the three relevant *IRAS* bands (see selection criterion number 4 above) will bias the sample towards objects of higher IR luminosity. Since many QSOs have pointed observations that have various detection limits, it is difficult to establish the luminosity limit that the selection criterion imposes on the sample. However, by inspecting the IR luminosities, L_{ir} , of the QSOs detected at these three bands, we find that objects out to $z \sim 0.1$ have a mean $\log L_{ir} \sim 11.5$, and those with $0.1 \lesssim z \lesssim 0.2$ have $\log L_{ir} \sim 11.7$ (a precise definition of L_{ir} is given in §4). Above redshifts $z \sim 0.25$, only ultraluminous ($\log L_{ir} \geq 12$) objects are detected at the three bands.

We use the B magnitudes published by Véron-Cetty & Véron (1996) as a starting point to select objects. However, these magnitudes are not homogeneous and have varying uncertainties which could, in some cases, push objects in or out of the sample. Therefore, in order to have as complete a sample as possible, we have considered all objects which satisfy every one of the other four selection criteria, and which have absolute B magnitudes up to one magnitude fainter than the cutoff magnitude. We then searched the literature for more accurate B magnitudes m_B and calculated new values of M_B (we assume $H_0 = 75 \text{ km s}^{-1} \text{ Mpc}^{-1}$ and $q_0 = 0.5$ throughout this paper) using $M_B = m_B + 5 - 5 \log D - k - A_B$, where D is the luminosity distance, $k = -2.5 \log (1 + z)^{1-\alpha}$ is the k correction (where we assume $\alpha = 0.3$), and A_B is the Galactic extinction, as given by Schlegel, Finkbeiner, & Davis (1998).

With the corrected values of M_B , there are only two objects in the pool that are fainter than, but within one magnitude of, the cutoff magnitude ($M_B = -22.1$) for our sample: Mrk 509, which is highly variable, but has an estimated $M_B = -21.7$ (B magnitude from Carone et al. 1996) and Mrk 231, also with $M_B = -21.7$ (B magnitude from Surace & Sanders 2000). There is much evidence indicating that the nucleus of Mrk 231 is heavily reddened, with more than 2 magnitudes of extinction in B (CS00b and references therein). In contrast, no evidence has been found for nuclear extinction in Mrk 509. In particular, in a spectropolarimetric study of Seyfert 1 galaxies, Goodrich & Miller (1994) find that there is ample evidence that the nuclear light of Mrk 231 is reddened and that the inferred scattering is from dust, while the weaker polarization in Mrk 509 is more likely due to electron scattering, and there is no evidence for nuclear reddening. Therefore we have chosen to include Mrk 231 in our sample since, except for the reddening, it would squarely fit in our sample. However, as Mrk 231 does not formally qualify as a bona fide QSO, it may be appropriate to leave it out in some analyses of the sample as a whole.

The final sample is listed in Table 1. The redshifts listed in this table are as measured from our spectra, with errors typically being ± 0.0001 . We have listed redshifts from the

Table 1. Transition Objects

Object Name	IAU	Redshift ^a	M_B ^b	25 μm^c	60 μm^c	100 μm^c
IRAS 00275–2859	0027–289	0.2792	–23.16	173±45	690±55	734±147
IZw 1	0050+124	0.0611	–22.62	1097±20	2293±17	2959±51
3C 48	0134+329	0.3694	–24.55	160±08	770±09	1080±27
Mrk 1014	0157+001	0.1634	–23.97	520±58	2377±56	2322±130
IRAS 04505–2958	0450–299	0.2863	–24.30	189±19	650±52	765±122
IRAS 07598+6508	0759+651	0.1483	–24.16	535±37	1692±85	1730±190
Mrk 231	1254+571	0.0422	–21.67	9184±11	35257±16	34229±47
PG 1543+489	1543+489	0.4009	–24.27	126±18	348±26	485±79
PG 1700+518	1700+518	0.2923	–25.00	220±21	480±36	482±88

^aQSO redshifts measured from our spectra, except for IZw 1 (Solomon et al. 1997), IR 07598+6508 (Lawrence et al. 1988), and Mrk 231 (Carilli et al. 1998)

^bValues of M_B account for Galactic reddening and k-corrections. We used B magnitudes taken from Véron-Cetty & Véron (1996) for IRAS 00275–2859 and IRAS 04505–2958; Elvis et al. (1994) for IZw 1 and 3C 48; Schmidt & Green (1983) for Mrk 1014, PG 1543+489, and PG 1700+518; Surace & Sanders (2000) for IRAS 07598+6508 and Mrk 231. The cutoff value for QSOs, as defined by Schmidt & Green (1983), is $M_B = -22.1$ for our chosen cosmology.

^cIRAS flux density values in mJy

literature as indicated in the table for three objects whose emission lines are heavily contaminated by Fe II emission. References for B magnitudes are as indicated in the table. The last three columns list the *IRAS* flux densities at 25 μm , 60 μm and 100 μm , respectively. Figure 1 shows the position of these objects in the FIR color–color diagram, indicated by open circles; the 22 other objects that satisfy selection criteria 1 through 4 are indicated by filled squares.

3. IRAS 00275–2859, IRAS 04505–2958, PG 1543+489, and I Zw 1

3.1. Observations and Data Reduction

Spectroscopic observations were carried out with the Low-Resolution Imaging Spectrometer (LRIS; Oke et al. 1995) on the Keck II telescope. We used a 300 groove mm^{-1} grating blazed at 5000 \AA with a dispersion of 2.44 \AA pixel^{-1} . The slit was 1" wide, projecting to ~ 5 pixels on the Tektronix 2048 \times 2048 CCD. We obtained two or three exposures for each slit position, dithering along the slit between exposures. In Table 2 we show a complete journal of observations, including slit positions, total exposure times, and the dates when the objects were observed.

The spectra were reduced with IRAF, using standard reduction procedures (see *e.g.*, CS00b for details). For IRAS 04505–2958, we subtracted the scattered light from the QSO from the spectrum of the companion galaxy by reversing the 2 dimensional spectrum and subtracting it from the original spectrum (the slit position was chosen so that there would be no light scattered from the star NE of the QSO in our slit). For IRAS 00275–2859, we subtracted a version of the QSO spectrum from those of the host galaxy, scaled according

Table 2. Journal of Spectroscopic Observations

Object	PA (deg)	Offset (arcsec)	Dispersion (\AA pixel^{-1})	Total Int. Time (s)	UT Date
IRAS 00275–2859	325.1	0.0	2.44	3600	98 Sep 13
IRAS 04505–2958	–21.0	1.0 E	2.44	3600	97 Oct 10
PG 1543+489	–30.0	4.9 S	2.44	2400	97 Jun 12
I Zw 1	36.6	~ 10 N	2.44	2400	97 Oct 10

to the amount of broad line contamination seen in the spectra. The same procedure was followed for the regions closer to the QSO in PG 1543+489, where we obtained a separate 300 s exposure of the QSO nucleus. No correction was needed for the spectra of IZw 1.

We have described our modeling strategy in detail elsewhere (CS97, SCC98, CS00a, CS00b). Briefly, we use Bruzual & Charlot (1996) isochrone synthesis models with solar metallicity and a Scalo (1986) initial mass function (IMF). We have previously (SCC98) found that the ages determined for the post-starburst populations are remarkably robust with respect to the different assumptions about the nature of the older stellar component. Here we use a 10-Gyr-old model with an exponentially decreasing star formation rate with an e-folding time of 5 Gyr as an old, underlying population. To this we add a young starburst model and do a χ^2 fit to the data to determine the best fitting age and relative contributions of the two populations. We have found (CS00a) that such age determinations typically have a precision of about $\pm 50\%$.

We obtained color maps of these objects prior to spectroscopic observations in order to choose slit positions. All imaging observations at optical wavelengths were done with the University of Hawaii 2.2 m telescope at f/10 using an Orbit CCD, which yielded an image scale of $0''.138 \text{ pix}^{-1}$. For IRAS 00275–2859 and IRAS 04505–2958, we used a U^* filter centered at 3874 \AA with a bandpass of 593 \AA to avoid strong emission lines, and we obtained six 1200 s exposures for each object. We also obtained four 900 s exposures and four 300 s exposures for each object, respectively, through a V filter, which included $H\gamma$ through He emission, but avoided the stronger $H\beta$, [O II] and [O III] emission lines. We obtained four 900 s B -band and three 600 s V -band images of PG 1543+489. Finally, we obtained five 1200 s exposures of IZw 1 through a U' filter (centered at 3410 \AA with a bandpass of 320 \AA), and six 300 s exposures through a B' filter (centered at 4648 \AA with a bandpass of 830 \AA), where both filters were chosen, once again, to avoid contamination from strong emission lines. All images were obtained in subarcsecond seeing and near photometric conditions, except for those of IZw 1, which were taken through cirrus.

Additionally, we obtained high-resolution near-IR images using the tip-tilt system at the f/31 focus of the University of Hawaii 2.2 m telescope. The 1024×1024 QUIRC (HgCdTe) infrared camera (Hodapp et al. 1996) gave a plate scale of $0''.0608 \text{ pixel}^{-1}$. We obtained a 16×300 s H -band image of IRAS 00275–2859, a 21×300 s H -band image of IRAS 04505–2958, a 10×600 s K' image of PG 1543+489, and a 76×60 s H -band image of IZw 1. Optical and near-IR images were reduced with IRAF using standard procedures.

HST WFPC2 images of IRAS 00275–2859 and IRAS 04505–2958 were obtained from the *HST* data archive. For IRAS 00275–2859 we used two Planetary Camera (PC1) 300 s exposures in the F606W filter, and two Wide Field Camera (WF3) 400 s exposures in the

F814W filter. For IRAS 04505–2958 we used one 400 s and two 600 s PC1 images in the F702W filter. We removed cosmic rays and combined images as described elsewhere (*e.g.*, CS00b).

For several objects, we estimate crude dynamical ages from tidal tail lengths. Although in one or two cases it might have been possible to estimate dynamical ages from other criteria, the tidal tail estimate can be applied to most of our sample, and we prefer to use the same criterion for consistency.

The projected physical length subtended by $1''$ is 3.5 kpc for both IRAS 00275–2859 and IRAS 04505–2958, 4.3 kpc for PG 1543+489, and 1.1 kpc for I Zw 1.

3.2. IRAS 00275–2859

IRAS 00275–2859 (shown in Fig. 2) was the second previously unidentified QSO discovered in the *IRAS* database (Vader & Simon 1987). The spectrum of the QSO (Fig. 3, bottom panel) shows broad Balmer emission lines at $z_{\text{QSO}} = 0.2792$, no narrow emission lines except for very faint [O II] $\lambda 3727$, and is otherwise dominated by strong Fe II emission.

IRAS 00275–2859 has been described as having a luminous host galaxy with a “clear tail” extending to the north-east and “two nuclei” separated by $\sim 2''$, the fainter of which has been interpreted as the nucleus of a strongly interacting galaxy. Thus, it has been concluded that this object is in a pre-merger stage (Vader et al. 1987; Hutchings & Neff 1988; Clements et al. 1996b; Zheng et al. 1999).

In the top panels of Fig. 2 we show an *HST* PC1 image of IRAS 00275–2859. It is evident from this low contrast image that the “second nucleus” is rather a bright knot ($M_R \sim -17.5$) $2''.7$ south-east of the QSO nucleus, and that it is part of a linear structure in a highly disturbed host. This knot is very bright in our $U^* - V$ color map in the bottom right panel of Fig. 2, and its spectrum (Fig. 3, middle panel) shows a blue continuum with strong emission lines at $z = 0.2781 \pm 0.0001$, with a velocity gradient of $\sim 140 \text{ km s}^{-1}$ from southeast to northwest. The strong emission lines include low ionization species such as He I $\lambda 5876$ and [N I] $\lambda\lambda 5198, 5200$. Emission line flux ratios indicate that the emission is most likely due to gas ionized by young stars rather than by the QSO (Veilleux & Osterbrock 1987). Thus, instead of being a “second nucleus,” the knot appears to be a giant (600 pc) H II region, roughly the size of 30 Doradus in the Large Magellanic Cloud (*e.g.*, Meylan 1993). This example illustrates that claims of second or multiple nuclei from morphological data alone (particularly ground-based imaging) should be taken with some caution.

Fig. 2.— Space- and ground-based images of IRAS 00275–2859. The *HST* PC1 F606W image (top left) shows diffuse clumps NW of the QSO; a spectrum of this area is shown in Fig. 3. The WFC3 F814W image (top right) highlights the curved extension on the NW. The high-contrast *HST* WFC3 (bottom left) and ground-based $U^* - V$ (bottom right) images have been smoothed to show the low surface brightness features. In $U^* - V$ map, darker regions indicate more negative values of $U^* - V$. The $4''$ scale bars (equivalent to 14 kpc) shown in the left-hand panels also apply to the corresponding panels to the right. In this and all subsequent images, north is up and east to the left.

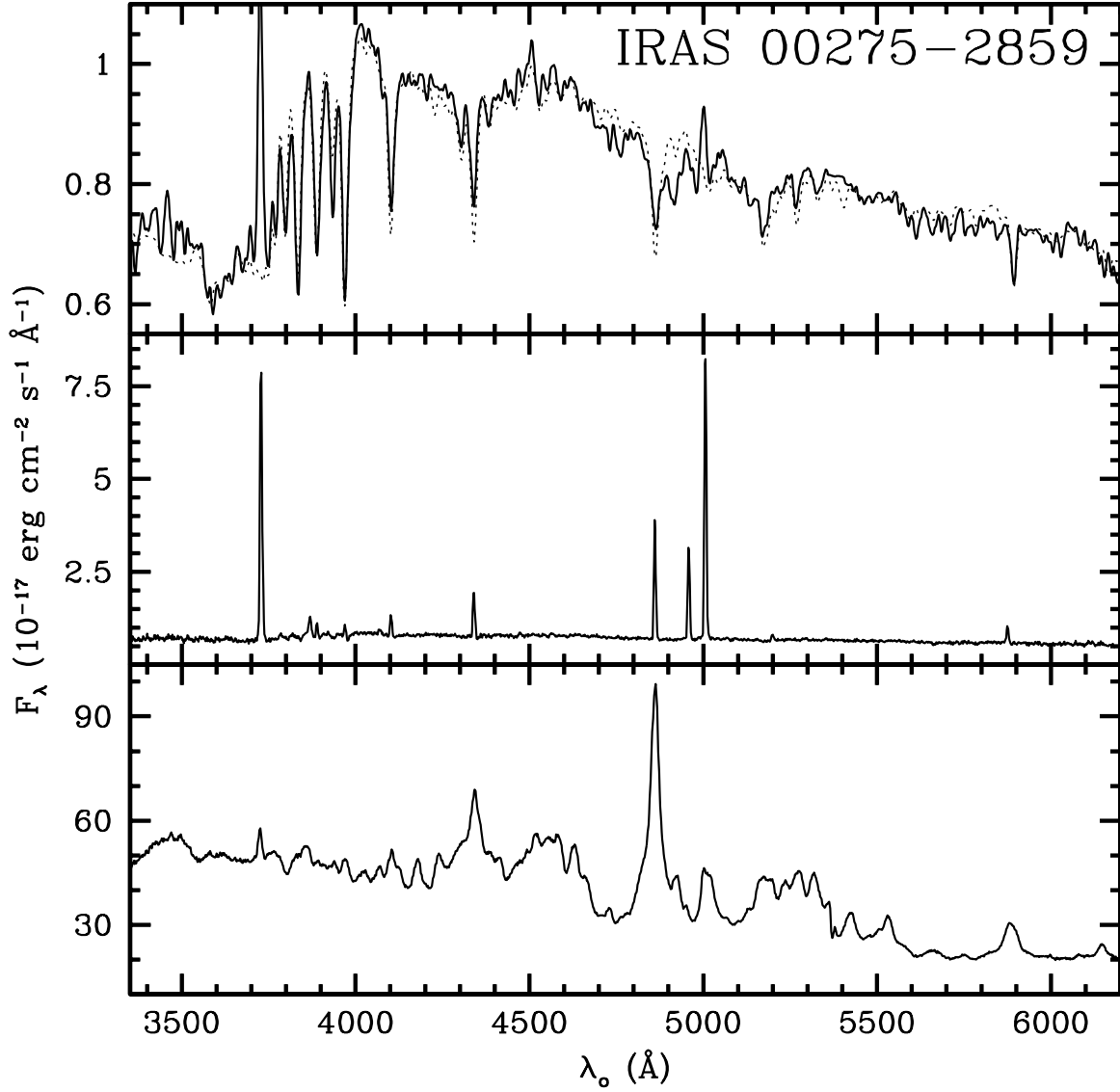


Fig. 3.— *Top* : Spectrum of the host galaxy of IRAS 00275–2859. The dotted line is a model formed by a 50 Myr old instantaneous burst model and an old underlying population. *Middle* : Giant H II region in host galaxy ~ 2.7 southeast of the QSO nucleus, previously identified as a secondary nucleus. *Bottom* : QSO. All spectra are in rest frame.

The *HST* PC1 image shows two or more diffuse clumps $\sim 1''.8$ northwest of the QSO. The spectrum of this region is shown in the top panel of Fig. 3; its redshift, measured from stellar absorption lines, is $z = 0.2804$. The starburst age obtained from modeling this region is 50 (+30, –20) Myr; the flux contribution from the old and young populations is roughly equal at rest frame 5000 Å. The spectrum of this region is characteristic of other regions in the host galaxy, excluding the H II region.

Our ground-based optical and near-IR images, as well as the *HST* WFPC2 images (Fig. 2, bottom panels) show clearly the tail on the east first reported by Vader et al. (1987). The tail is $\sim 12''$ or ~ 40 kpc long, and it extends roughly from the position of the H II region towards the east and north. The tail appears redder than the host galaxy in the $U^* - V$ image (Fig. 2), and this may indicate that the tail is predominantly made of older stars, as suggested by Hutchings & Neff (1988). The tail shows, however, several blue clumps, possibly regions of star formation like those seen in the tidal tails of nearby merging galaxies and of 3C 48 (CS00a) and Mrk 1014 (CS00b).

A plausible second tail is visible in the *HST* WFPC2 image as well. This tail extends for $\sim 11''$ from the northwest of the QSO (including the clumps described above) and arches towards the west and southeast, staying close to the host galaxy, and ending in the faint extension southeast of the H II region. This faint extension has a much higher approaching velocity (-600 ± 200 km s $^{-1}$) than that of the adjacent brighter region closer to the QSO (-190 ± 100 km s $^{-1}$) with respect to the central and north regions of the host galaxy. It appears then that the putative second tail has a high inclination angle with respect to the plane of the sky, and that the system has some rotation about an axis perpendicular to the bright linear feature in the host. This linear feature, which is also evident in near-IR images, may indicate that the main body of the host galaxy is also seen at a high inclination.

Thus, the host galaxy of IRAS 00275–2859 appears to be in the late stages of a merger of two disk galaxies. Assuming a projected velocity of 300 km s $^{-1}$ on the plane of the sky, the tidal tails have dynamical ages of 130 Myr each. The peak of star formation in the host galaxy seems to have occurred well after the tails were first launched, as was the case in 3C 48 (CS00a), Mrk 1014, and IRAS 07598+6598 (CS00b).

3.3. IRAS 04505–2958

The luminous, $z = 0.286$, radio-quiet QSO IRAS 04505–2958 was first detected by *IRAS*, identified as an AGN candidate by de Grijp, Miley, & Lub (1987), and spectroscopically identified as a QSO by Low et al. (1988). Optical images by Hutchings & Neff (1988)

Fig. 4.— *HST* PC1 F701W (left) and *H*-band (right) images of IRAS 04505–2958. The 4'' scalebar is equivalent to 14 kpc.

showed a “double nucleus” separated by 2'', and “a suggested linear tail along the line of the nuclei, to the SE”. Later it was found that the second “nucleus”, the one to the northwest, was instead a foreground G star (Low et al. 1989). The “linear tail” to the southeast, however, was found to be a “ringlike feature” 1''.5 from the nucleus in a *HST* F702W PC1 image by Boyce et al. (1996) and interpreted as a galaxy that has violently interacted with the QSO host galaxy. In Fig. 4 we show a lower contrast version of the archival *HST* PC1 image, which shows more clearly the structure of the ring galaxy.

Figure 5 shows the spectrum of the ring galaxy. The spectrum is dominated by strong Balmer absorption lines; the $H\beta$ and oxygen narrow emission lines most likely come from extended gas ionized by the QSO and not from star forming regions. We obtain an age of 128 (+100, –64) Myr for the starburst population, which contributes $\sim 4.5\%$ of the total luminous mass along the line of sight.

It has been found that different individual star forming knots within any given collisional ring galaxy have virtually no spread in ages (Bransford et al. 1998), which is to be expected if the star formation was triggered by the propagation of a radial density wave at the time of collision (Lynds & Toomre 1976). We therefore expect the age determined from the integrated spectrum of the companion to IRAS 04505–2958 to be fairly representative of the starburst activity in the companion.

The companion galaxy is clearly visible in our high resolution *H*-band image (Fig. 4, right panel) as a slightly elongated feature, with a faint extension to the southwest corresponding to the tidal tail seen in the *HST* image. This tail extends for ~ 16 kpc from the south of the companion and arching towards the northwest. The size of the brightest part of the ring as measured from both the F702W image and the *H*-band image is $\lesssim 4.3$ kpc.

The redshift of the ring galaxy is $z_{\text{comp}} = 0.2865 \pm 0.0002$ as measured from absorption lines, and that of the QSO is $z_{\text{QSO}} = 0.2863 \pm 0.0002$ as measured from broad and narrow emission lines. The low relative velocity between the QSO and companion may indicate that the companion is near apocenter, if the plane of the orbit between the galaxies is at high inclination (as suggested by the morphology of the companion: since we see the ring in a fairly open position, and a ring galaxy can be produced only by a passage with a high inclination to the plane of the original disk, the mutual orbit is likely to be well out of the plane of the sky). Using the tail of the companion to estimate the time elapsed since the collision, we obtain ~ 50 Myr, which is less than the starburst age. The difference between

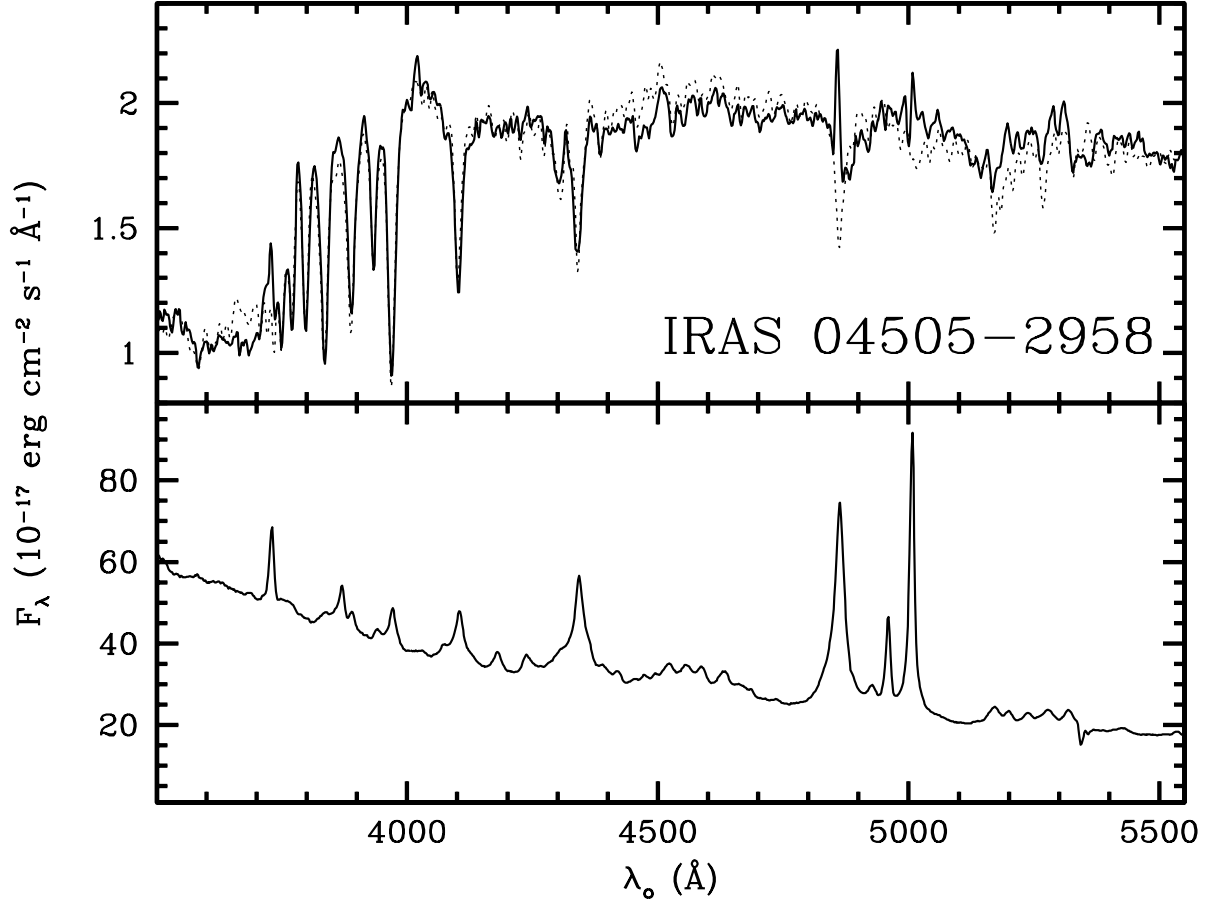


Fig. 5.— *Top* : Rest frame spectrum of the companion galaxy to IRAS04505–2958. The dotted line is a model formed by the sum of a 128 Myr old starburst and an old underlying population. *Bottom* : Rest frame spectrum of the QSO.

these ages is similar to that of PG 1700+518, where the dominant post-starburst population has an age of 85 Myr, but the dynamical age of the tail of the companion (estimated using similar assumptions) is only ~ 40 Myr. This lends additional support to the suggestion by Hines et al. (1999b) that these two systems have undergone very similar interactions, both with small impact parameters.

Fig. 6.— V -band and K' images of PG 1543+489. Both images have been smoothed to show the low surface brightness features more clearly. Scalebar is 43 kpc.

3.4. PG 1543+489

The radio-quiet QSO PG 1543+489 (Fig. 6) has a redshift $z_{\text{QSO}} = 0.4009 \pm 0.0001$ as measured from the $H\beta$ and $H\gamma$ broad emission lines. The QSO spectrum (bottom panel of Fig. 7) shows strong Fe II emission, and no narrow emission lines.

Turnshek et al. (1997) list PG 1543+489 as one of 18 candidate low-redshift BAL QSOs based on the QSO’s [O III] and Fe II emission properties. They note that while the *IUE* spectrum of PG 1543+489 (Lanzetta, Turnshek, & Sandoval 1993) has very poor signal-to-noise, it appears somewhat absorbed, so that it remains possible that this object may be a BAL QSO (Turnshek et al. 1997).

Figure 6 shows the QSO and a compact nearly stellar object $6''$ (25.3 kpc) south of the QSO. A bridge between both objects is visible in the V -band image, but only the smaller clump on the west edge of the bridge is visible in the K' image.

The spectrum of the companion (Fig. 7, top panel) shows that it is a galaxy with a stellar continuum and absorption and emission lines at a redshift $z_{\text{comp}} = 0.4004 \pm 0.0002$, which corresponds to a velocity difference of $110 \pm 60 \text{ km s}^{-1}$ with respect to the broad line region in the QSO. The steep Balmer emission line decrement indicates that the companion suffers from dust extinction along the line of sight.

If we assume that the extinction is caused by a screen of dust located between us and the companion galaxy, the Balmer line ratios indicate an extinction $A_v \sim 1.9$. Using this very rough estimate, we corrected the spectrum of the companion assuming a Galactic extinction law (Cardelli, Clayton, & Mathis 1989), and subtracted the Balmer emission lines assuming Case B recombination. The resulting spectrum is shown in the middle panel in Fig. 7. Modeling this spectrum with our usual method yields a starburst age of 130 Myr. This age is highly uncertain since we have used very rough and simple assumptions to correct for reddening, and we also note that the model clearly diverges from the observed spectrum at short wavelengths. However, it is clear that the companion galaxy has a post-starburst spectrum, and the weakness of the Ca II, G-band, and Mg Ib features indicates that its age cannot be much greater than ~ 200 Myr.

We have a very faint spectrum of the southwest edge of the host galaxy of PG 1543+489. Unfortunately, the spectrum is too noisy to show stellar features. After correction for scattered QSO light, its SED is similar to that of the companion galaxy, although it appears

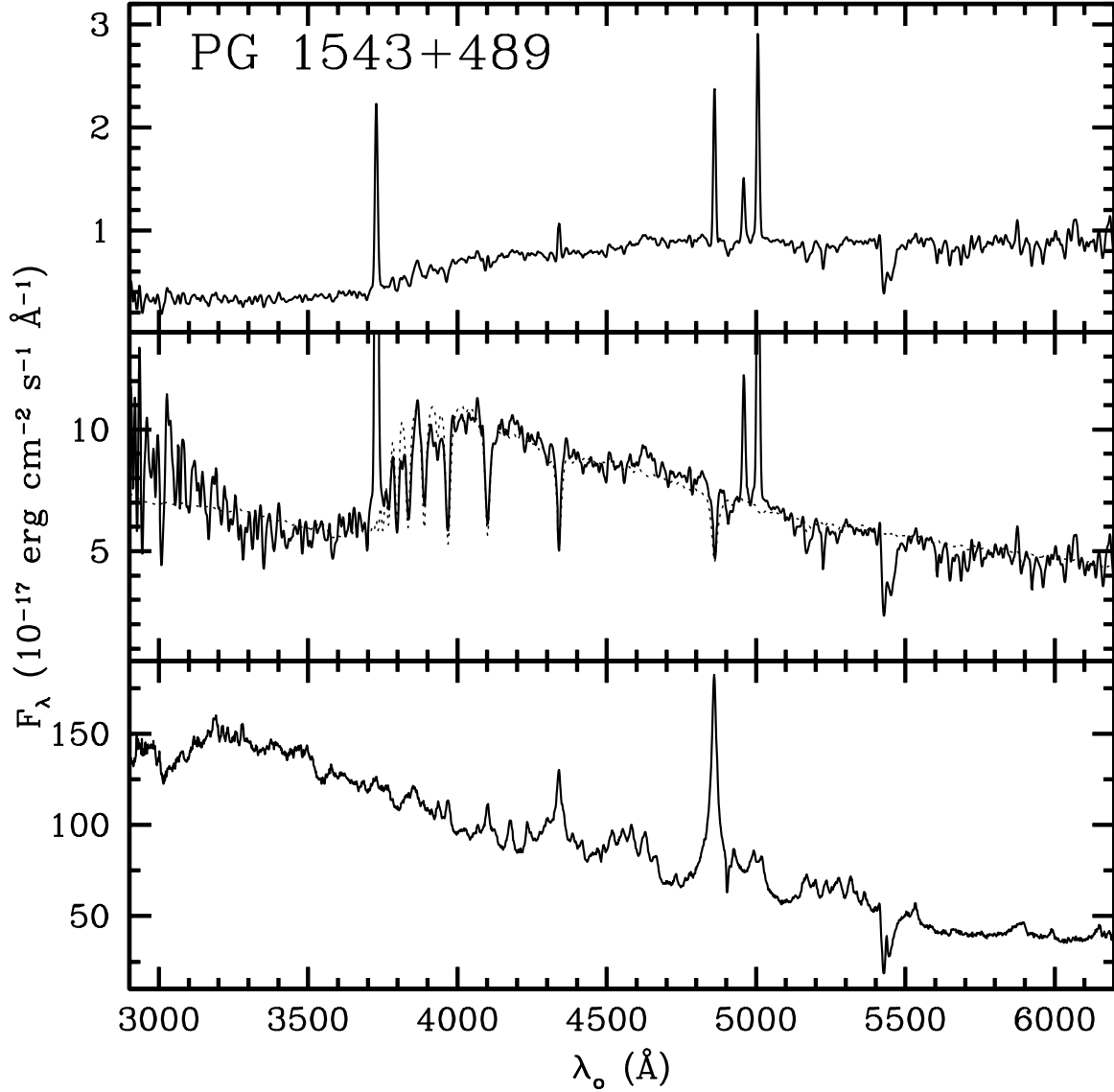


Fig. 7.— *Top*: Rest frame spectrum of the companion galaxy to PG 1543+489. *Middle*: Same spectrum, but dereddened by $A_v = 1.9$ and with Balmer emission lines subtracted assuming Case B recombination. The dotted line is a model formed by a 130 Myr old instantaneous burst model and an old underlying population. *Bottom*: Rest frame spectrum of the QSO. The absorption feature near 5450 \AA in all panels is the atmospheric B-band.

to be slightly bluer. Faint [O II] and [O III] emission is visible in a small clump along the bridge $\sim 2''$ away from the companion.

The small projected distance and relative velocities between the QSO and the companion, the bridge connecting both objects, and the dominant post-starburst population in the companion galaxy (and possibly in the QSO host) are all indicative of a strong interaction between these two objects. The companion galaxy appears as a very compact object (≤ 1.7 kpc) in our $0''.35$ seeing near IR images. What we are seeing is perhaps the tidally stripped core of the interacting galaxy like those proposed by Stockton (1982). Even without correcting for extinction, the companion has nearly an L^* luminosity, and the corrected luminosity is likely to be at least a few L^* , which is comparable to those of the companions to PG 1700+518 (Hines et al. 1999b) and IRAS 04505–2958 (Boyce et al. 1996). Thus, the companion to PG 1543+489 and the host are likely to merge shortly, resulting in a major merger.

3.5. I Zw 1

IZw 1 ($z = 0.061$) is near the lower limit of the luminosity cutoff for QSOs defined by Schmidt & Green (1983), and it is often classified as a Seyfert 1 galaxy. The nuclear spectrum of IZw 1 shows strong Fe II emission and weak forbidden-line emission (Sargent 1968; Boroson & Oke 1987).

The host galaxy of IZw 1 shows what appear to be two spiral arms, as well as two “companion” objects (Fig. 8; see also, *e.g.*, Bothun et al. 1984; Surace et al. 1998; Zheng et al. 1999). Stockton (1982) reported that the object to the north is a projected star, while the one to the west is a true companion with stellar features. The $U' - B'$ color map shown in the lower-left panel of Fig. 8 shows large, blue clumps along the arms. We have obtained spectra of the companion galaxy and the northwest arm of the host galaxy.

Fig. 9 shows the spectrum of the brightest clump along the arm, which is characteristic of the spectra in different regions along the arm (this clump is at a position angle of about -60° from the nucleus of IZw 1, close to a point a little less than halfway along a line joining the companion to the star indicated in Fig. 8). The spectrum shows strong emission lines superposed on a stellar continuum. We measured line flux ratios from lines that are close in wavelength (hence fairly insensitive to reddening; Veilleux & Osterbrock 1987) and found that they are consistent with emission coming from H II regions. As in the case of the companion to PG 1543+489, the steep Balmer decrement indicates extinction from dust along the line of sight. Using the assumptions described in §3.4, we corrected for extinction

Fig. 8.— Top: U' (left) and B' (right) images of IZw 1. The U' image has been smoothed with 0.5 pixel σ gaussian to show the low surface brightness features more clearly. Bottom: $U' - B'$ color map (left) and high contrast B' image (right). Scale bar shown in upper-left panel applies to both upper panels and lower-left panel, and is equivalent to 11 kpc.

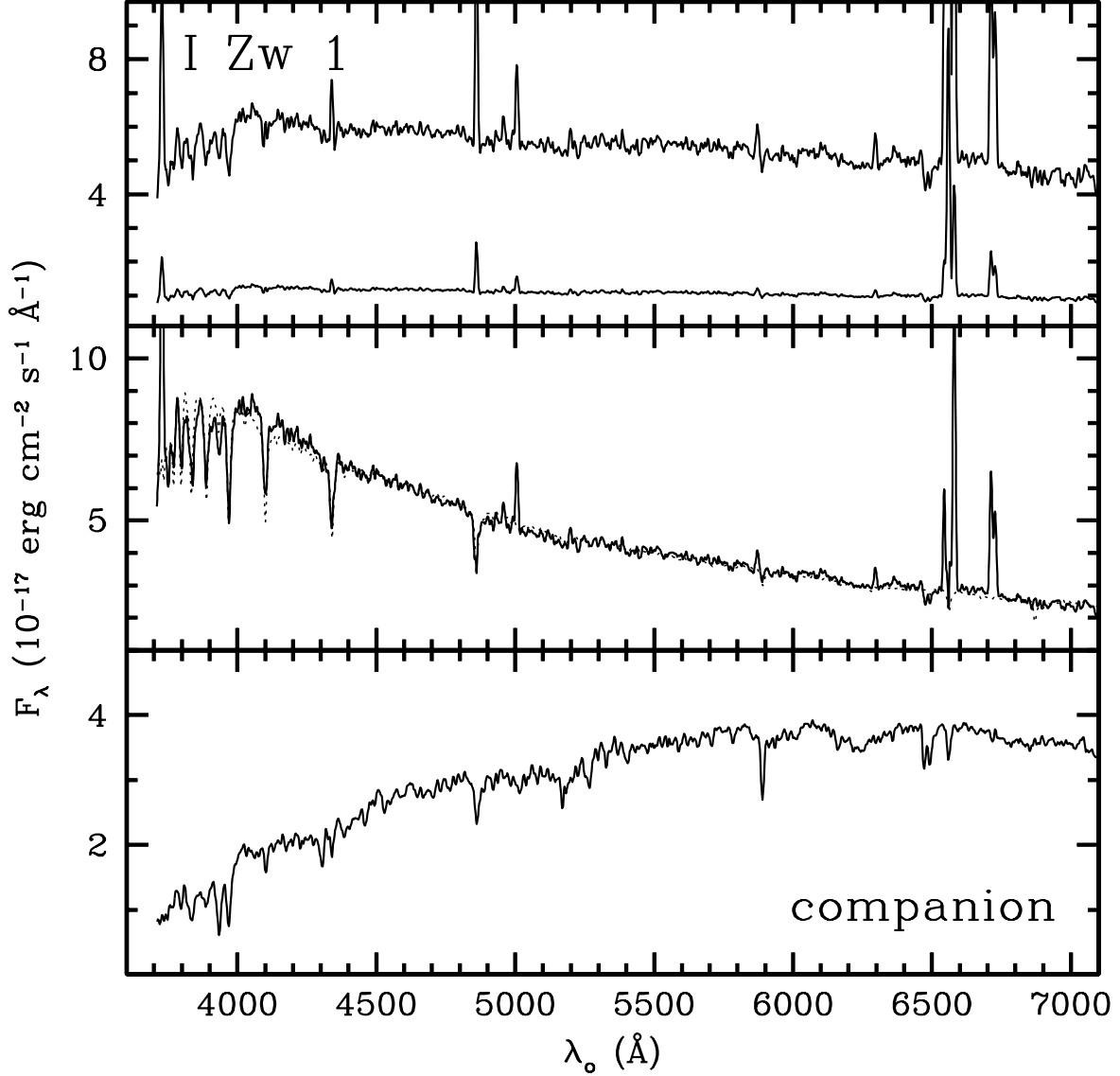


Fig. 9.— *Top* : Spectrum of an H II region in host galaxy of I Zw 1 (lower trace). The upper trace displays the same spectrum, scaled by a factor of 5. *Middle* : Same spectrum, but corrected for $A_v = 1.4$ and with Balmer emission subtracted, assuming Case B recombination. The age of the starburst, determined from the model (dotted line), is 4 Myr. *Bottom* : Companion galaxy to I Zw 1. All spectra are in rest frame. The absorption feature near 6500 Å in all panels is the atmospheric B-band.

and subtracted emission lines. The resulting spectrum is shown in the middle panel of Fig. 9, where we also plot a model resulting from a 4 Myr starburst and an old underlying population. This age is very uncertain, given the assumptions we have made to correct the spectrum and the fact that we do not have the blue side of the spectrum (see section on Mrk 231 in CS00b). In any case, this age is consistent with the presence of H II regions and, as we have mentioned in CS00a,b, such a young age is simply indicative of continuous ongoing star formation.

The spectrum of the companion galaxy 15''6 or 16.7 kpc west of the QSO (Fig. 9, bottom panel) shows the stellar absorption features of an old population at a redshift $z_{\text{comp}} = 0.0616 \pm 0.0001$, which, compared with the redshift of the host, $z_{\text{host}} = 0.0610 \pm 0.0003$, yields a relative velocity of $170 \pm 110 \text{ km s}^{-1}$. The spectrum does not show any signs of recent star formation, and it is in fact reasonably fit by a 13 Gyr single burst population model, assuming there is no significant reddening due to dust.

IZw 1 shows a seemingly normal disk galaxy harboring a QSO and intense star formation, and with strong evidence of a nuclear starburst ring (Schinnerer, Eckart, & Tacconi 1998). However, the role of a tidal interaction is uncertain. The morphology of the host galaxy is not indicative of a strong interaction like those seen in the rest of the objects in our sample. In addition, the profiles of CO and H I lines of the host galaxy are double-horned and symmetric like typical rotating disks in spiral galaxies (Bothun et al. 1984; Barvainis Alloin), and VLA 21 cm H I emission images of the host show a nearly unperturbed rotating disk (Lim & Ho 1999). The companion galaxy, on the other hand, appears to be at least weakly interacting with the host. The low relative velocities indicate that the companion may be tidally bound to the QSO. Our deep B' image shows an extended distribution of very low surface brightness emission, with the edge of the distribution close to the companion (Fig. 8, lower-right panel). Further, HI images show an extension in the disk of the host both toward and away from the companion galaxy (Lim & Ho 1999), which is often regarded as the classic signature of tidal interactions (Toomre & Toomre 1972). Our H -band image of the companion (not shown) shows a faint extension away from the host, roughly in the same direction that the HI disk is elongated (see Fig. 1 of Lim & Ho 1999). Thus, IZw 1 appears to be interacting with its companion galaxy. However, the interaction has not produced a burst of star formation in the companion (as was the case for PG 1700+518, IRAS 04505–2958, and PG 1543+489).

One possibility is that IZw 1 is in the process of accreting the low-mass companion (*i.e.*, a minor merger in progress), and that the host has developed the two-armed spiral pattern in response to the tidal perturbation, as shown in numerical simulations (Mihos & Hernquist 1994). Simulations also show that such interactions are also capable of triggering substantial

star formation when the central gas density becomes very large, shortly after the spiral arms form and while the companion is still separate from the host, if the host lacks a substantial bulge.

4. Summary of Properties of the Sample of Transition Objects

Table 3 summarizes the observed and derived properties of all the objects in the sample. Column 1 lists the name of each object, and column 2 its redshift as in Table 1. Column 3 lists $\log(L_{\text{ir}})$ in units of solar bolometric luminosity $L_{\odot} = 3.83 \times 10^{33} \text{ erg s}^{-1}$. We have calculated $L_{\text{ir}} = L(8-1000\mu\text{m})$ according to Sanders & Mirabel (1996), using $L_{\text{ir}} = 4\pi D_L^2 F_{\text{ir}}$, where D_L is the luminosity distance in cm, and $F_{\text{ir}} = 1.8 \times 10^{-11} (13.48f_{12} + 5.16f_{25} + 2.58f_{60} + f_{100})$ [$\text{erg s}^{-1} \text{ cm}^{-2}$], with $f_{12}, f_{25}, f_{60}, f_{100}$ being the *IRAS* flux densities in Jy given in Table 1. Objects with $\log(L_{\text{ir}}/L_{\odot}) > 11$ are considered luminous infrared galaxies (LIGs), and those with $\log(L_{\text{ir}}/L_{\odot}) > 12$, ultraluminous infrared galaxies (ULIGs).

Column 4 lists the ratio $\nu f_{\nu}(60\mu\text{m})/\nu f_{\nu}(B)$, where $f_{\nu}(B) = 10^{-0.4(B+48.36)} [\text{erg cm}^{-2} \text{ s}^{-1} \text{ Hz}^{-1}]$ (Schmidt & Green 1983), using the *B* magnitudes described in §2.1. This quantity gives a rough measure of the ratio of the SED at IR to optical wavelengths.

The starburst peak age given in column 5 is the predominant starburst age found in the host galaxy or companion (see §3, CS97, CS00a, CS00b). We have arranged the objects in order of increasing peak age. The age of IZw 1 appears in parenthesis to indicate our uncertainty whether the star formation found has been induced by tidal interaction as in the other objects. Column 6 lists the range of starburst ages found in objects with resolved galaxies. Column 7 indicates the kind of tidal interaction that each system is undergoing, as well as the merging stage for those which are major mergers. Column 8 gives a rough estimate for a dynamical age, in each case assuming a projected velocity of 300 km s^{-1} , and using the length scales as described for each object (§3, CS97, CS00a, CS00b). Because of projection effects and other uncertainties, these estimates will have typical errors of about a factor of 2. The dynamical age for PG 1543+489 appears in parenthesis since we used the length of the bridge between the QSO and the companion as the relevant length scale rather than the size of a tidal tail.

Columns 9 and 10 refer to the [O III] $\lambda 5007$ emission from gas ionized by the QSOs. Column 9 lists the rest-frame equivalent widths (REW) measured in the nuclear spectra of the QSOs. As we do not have a nuclear spectrum of IZw 1, we have taken the REW given by Boroson & Meyers (1992). Objects with $\text{REW}_{[\text{O III}]} < 5 \text{ \AA}$ are considered weak [O III] QSOs (Turnshek et al. 1997). Column 10 indicates whether each object shows luminous

Table 3. Summary of Properties of “Transition” Objects

Object Name (1)	QSO Redshift ^a (2)	$\log L_{ir}$ $/L_{\odot}$ (3)	νf_{60} $/\nu f_B$ ^b (4)	Starburst ^c Peak Range (5) (6)		Tid Int ^d (7)	Dyn Age ^c (8)	[OIII] Nucl. ^e (9)	Ext. (10)	Fe II $/H\beta$ ^f (11)	Low BAL (12)
IZw 1	0.0611	11.87	1.98	(4)	...	3	...	20	N?	1.5	N
3C 48	0.3694	12.81	3.85	9	0—114	1	200	49	Y	1.0	N
IR 07598+6508	0.1483	12.41	2.03	32	32—70	1	160	0	w	2.6	Y
Mrk 231	0.0422	12.50	34.65	42	0—360	1	110	0	N?	2.1	Y
IR 00275–2859	0.2792	12.54	7.19	50	0— 50	1	130	0	N?	1.2	?
PG 1700+518	0.2923	12.58	1.00	85	...	2	40	2	w	1.4	Y
IR 04505–2958	0.2863	12.55	2.50	128	...	2	50	42	w?	0.8	?
PG 1543+489	0.4009	12.67	1.38	<200	...	2	(80)	0	N	1.2	?
Mrk 1014	0.1634	12.52	4.13	240	180—290	1	330	57	Y	1.0	N

^aQSO redshifts measured from our spectra, except for I Zw 1 (Solomon et al. 1997), IR 07598+6508 (Lawrence et al. 1988), and Mrk 231 (Carilli et al. 1998)

^b $f_{60} = f_{\nu}(60\mu\text{m})$ and $f_B = f_{\nu}(0.44\mu\text{m})$

^cStarburst and dynamical ages in Myr.

^dType of tidal interaction. 1: major merger, nuclei have already merged. 2: Galaxies are still distinct and are likely to result in a major merger. 3: Host interacting with low-mass companion.

^eRest equivalent width in Å. Values given include anomalous narrow emission in 3C 48 (CS00a) and blue wing in Mrk 1014 extending to $\sim -1500 \text{ km s}^{-1}$. REW for I Zw 1 from Boroson & Meyers (1992)

^fValues of Fe II $\lambda 4570/H\beta$; see text for references.

extended emission-line regions. A “w” indicates that the object shows only a much weaker, relatively less extended emission. The classification is based on the emission observed in our 2-dimensional long-slit spectra of the objects, and confirmed by our [O III] images of 3C 48 (CS00a) and IRAS 07598+6508 (CS00b), and results published by Stockton & MacKenty (1987) for PG 1700+518, PG 1543+489, and Mrk 1014. Our classification for the remaining four objects is uncertain (as indicated by question marks) since we do not have imaging information, and our slit positions could have missed regions of strong emission.

Column 11 gives the ratio of the flux of the Fe II complex $\lambda\lambda 4500\text{--}4680$, formed by multiplets 37 and 38, to the flux of $H\beta$. This Fe II complex (usually referred to as Fe II $\lambda 4570$) is often used in measuring ratios since it is the easiest and most reliable blend to measure, and its proximity in wavelength to $H\beta$ minimizes the effects of reddening and uncertainties in the flux calibration. Whenever possible, we have listed those ratios found in the literature where it is clear that the authors have subtracted the Fe II emission before measuring the $H\beta$ flux. These values are close to the values we obtain by simply deblending the lines in our spectra, except in the case of I Zw 1, for which we do not have a nuclear spectrum. The references for the ratios we list are: Boroson & Green (1992) for I Zw 1 and PG 1700+518; Joly (1991) for 3C 48; L ipari (1994) for IRAS 07598+6508, Mrk 231, and IRAS 00275-2859. We have listed ratios measured from our spectra for the remaining three objects. Objects with $\text{Fe II } \lambda 4570/H\beta > 1$ are considered strong Fe II emitters, while those with ratios > 2 are called extreme Fe II emitters (L ipari 1994).

Finally, column 12 indicates whether the QSO spectrum of each object shows low-ionization broad absorption lines (BAL). Objects with question marks either do not have published UV spectra, or (in the case of PG 1543+489) their spectra do not have enough signal-to-noise to clearly indicate whether the object is a BAL QSO.

As can be seen from Table 3, the sample appears to be very homogeneous. The selection criteria ensured that these objects would have similar far infrared colors. However, we have found that these objects share many other properties. All objects are involved in tidal interactions, and most of them are the result of major mergers, completed or in progress. The stellar populations are very similar in the different galaxies, with a very small range of interaction-induced starburst ages. In addition, we find a large incidence of objects with weak [O III], BAL spectra, and strong Fe II emission.

In the following section, we will consider each one of these properties individually. For each property, we will provide some background, and describe and discuss our results. In §6 we will put all things together and propose scenarios that incorporate all of our results; we will also consider the question of evolution.

5. Discussion of Individual Properties

5.1. Stellar Populations and Interaction Histories

We have found that 8 out of 9 objects in the sample have unambiguous tidal interaction-induced post-starburst populations. Of the seven objects that show tidal tails, we find knots of star formation along the tails, as predicted by numerical simulations, in at least four cases, and perhaps six. We also find enhanced star forming activity in the leading edges of the tails of two of the objects. Regions of star formation are found throughout the host galaxies and, at least in the 5 cases where we have high spatial resolution, the strongest and youngest starbursts are invariably concentrated towards the center of the host galaxy, clearly indicating the concentration of material towards the nucleus expected in mergers.

As discussed in detail in CS00b, this concentration of material towards the nucleus is likely to have triggered the central strong starbursts and the QSO activity roughly simultaneously, but we are unable to observe these initial central starbursts because they are hidden both by the bright QSO nucleus and by possible more recent starburst activity. We have chosen to use a “peak” starburst age (column 5 in Table 3) as a measure of the age of the QSO activity. This peak age is the age at which we find evidence for strongest starburst activity in a given host galaxy, but this is somewhat subjective. As we have seen, there is an unavoidable uncertainty in using starburst ages to place QSOs in a time sequence. This is aggravated in our sample by the fact that we have such a small range of starburst (as well as dynamical) ages in the host galaxies. Take the case of Mrk 231 (see CS00b): did the onset of the QSO activity occur ~ 300 Myr ago, when the first starbursts were ignited, or was it more recently, less than 5 Myr ago, the time when the star formation in the large H II region to the south and possibly in the knots near the nucleus started? If we are to take the range of starburst ages in a given host galaxy (column 6 in Table 3) as the uncertainty in the age of the QSO activity, then this uncertainty is almost as large, in some cases, as the difference in ages between the oldest and the youngest of the nine objects.

While the starburst ages may not accurately pinpoint the age of the QSO activity, they are fairly representative of it. Simple arguments can show that the age of the QSO activity can be neither much younger nor much older than the starburst ages. As we have seen, the starburst ages are consistent with having been induced by the evident tidal interactions. To say that the starbursts came much later than the QSO activity is then to say that galaxies already hosting QSOs were involved in major mergers that resulted in unusual levels of star forming activity. While this may very well be possible, it is certainly *not probable*, as we will see in detail in §5.2. On the other end, we know that starbursts did not come much earlier than the QSO activity, since the starburst ages are already so young.

We have 5 confirmed major mergers in our sample, and three additional cases of strong interactions between galaxies of comparable size which are likely to merge in the near future. Only in one case do we have a possible ongoing minor merger, *i.e.*, an accretion of a low-mass companion by the host galaxy. Thus, major mergers are the most common triggering mechanism for the QSOs in our sample. Similarly, the presence of tidal tails in at least 7 of the objects in the sample implies that disk galaxies are often involved in these mergers. Whether the parent population of the QSO hosts themselves are usually disk galaxies is less certain. Clearly some are, since at least 3 of our sample show double tails, and I Zw 1 is definitely a spiral.

In terms of merger stage, we have 2 main groups: (1) objects whose nuclei have already merged, and (2) objects where the interacting galaxies are still distinct (column 7 of Table 3). By comparing the peak and range of starburst ages to the dynamical age of each of these objects, we find a distinction between the two groups: except for Mrk 231, every object in group 1 has starburst ages that are younger than their dynamical ages, while those of group 2 are older than their corresponding dynamical ages. This is consistent with the idea that objects in group 1 had some mechanism (possibly a significant bulge in at least one of the galaxies; Mihos & Hernquist 1996) to stabilize the gas against early dissipation, whereas objects in group 2 lacked this mechanism. The range of ages in Mrk 231 may indicate that this object was initially like those of group 2, but that we are seeing it at a time when the galaxies have already merged. The fact that we do not see any pre-merger systems (group 2) where the tidal tails precede the starburst activity in the hosts suggests that the strong peak starburst activity and the ignition of the QSOs in objects that do have a stabilizing mechanism is delayed until the later stages of the merger, in agreement with numerical models Mihos & Hernquist 1996). The fact that we see QSO activity in both groups is further evidence that the age of the QSO activity is more closely tied in with the starburst ages than with the morphology of the merger. It is clear, however, that the force of these conclusions is limited by the size of our sample and by the large uncertainties in the dynamical ages.

These results unambiguously indicate that we have a population of very young objects, both dynamically and in their stellar populations, and, as discussed above, with recently triggered QSO activity as well. We now need to consider other properties in this context.

5.2. QSOs and ULIGs: Chance Overlap?

We have confirmed the long suspected fact that the kind of FIR colors in the objects in our sample are indeed indicative of strong star formation in the host galaxies of QSOs. We

have also shown that the star formation is not confined to the central regions, but extends at some level over most of the host galaxies. These starbursts have been triggered by mergers rather than by the interaction of some kind of outflow from the QSO with the surrounding environments, even in the central regions (at least initially).

ULIGs are defined as galaxies with $\log(L_{ir}/L_{\odot}) > 12$, and their most common characteristic is that they are mergers: the merger rate in ULIGs is thought to be at least $\sim 95\%$ (Sanders & Mirabel 1996 and references therein). The other common characteristic is the intensified star formation as a result of the merger. So, an object that has an infrared luminosity $\log(L_{ir}/L_{\odot}) > 12$, widespread starbursts, and is a merger, is unambiguously a “bona fide ULIG”. Excluding Mrk 231 from our sample (on the grounds that its reddened B magnitude disqualifies it as a bona fide QSO), we have a sample of 8 bona fide QSOs, 7 of which are bona fide ULIGs as well (see Table 3).

If the QSO and ULIG were two completely unrelated phenomena, what is the probability that both would occur in a given galaxy by chance? In order to estimate this probability, we consider the space densities (Φ) of each of these two types of objects as compared with normal galaxies¹. We transform the different luminosity functions (LF) to bolometric luminosities to allow for meaningful comparisons between the different sets of objects (Soifer et al. 1987; Sanders & Mirabel 1996). For normal galaxies, we obtain a $\Phi \approx 3 \times 10^{-3} \text{ Mpc}^{-3}$ by integrating the Schechter LF for bolometric luminosities $10 \leq \log(L_{bol}/L_{\odot}) \leq 11.2$. The value $\log(L_{bol}/L_{\odot}) = 10$ corresponds roughly to L^* if its corresponding $M_B^* = -19.7$ is transformed to L_{bol} using the corrections described by Soifer et al. (1986), and 11.2 is where the LF virtually ends. For ULIGs, we use the LF given by Kim & Sanders (1998), corrected for a redshift $z = 0.4$, and assuming a density evolution proportional to $(1+z)^{\alpha}$, where $\alpha = 7.6$. For objects with $12 \leq \log(L_{bol}/L_{\odot}) \leq 13$, we obtain $\Phi \approx 1.7 \times 10^{-7} \text{ Mpc}^{-3}$ (here we have assumed that $L_{bol} \approx L_{ir}$; see Soifer et al. 1987). Finally, we use the LF for QSOs given by Grazian et al. (2000) in the range $11.2 \leq \log(L_{bol}/L_{\odot}) \leq 13.3$ (roughly equivalent to $-22.1 \leq M_B \leq -27.6$) and obtain a $\Phi \approx 2.2 \times 10^{-7} \text{ Mpc}^{-3}$. Thus, the fractions for ULIGs and QSOs are, respectively, 5.6×10^{-5} and 7.3×10^{-5} . Using these values, the probability that both phenomena will occur by chance in any given otherwise normal galaxy is 4.1×10^{-9} .

We now consider the expected number of galaxies that show both phenomena by chance

¹Since we are arguing that QSOs and ULIGs are both rare when compared to normal galaxies, we make conservative assumptions that lead to a lower space density for normal galaxies and higher space densities for QSOs and ULIGs. Thus (1) we assume that QSOs and ULIGs can only occur in galaxies of L^* and above; (2) we use a ULIG luminosity function corrected for the upper end of our redshift bin, and (3) we use a luminosity function for QSOs consistent with a luminosity dependent luminosity evolution, which leads to a Φ a factor of 3 higher than that estimated by the PG survey.

in the integrated comoving volume out to $z = 0.4$. Following Carroll, Press, & Turner (1992), the integrated comoving volume, V_C , from the present to a redshift z for an Einstein–de Sitter Universe is simply given by

$$V_C = \frac{4\pi}{3} \left(\frac{c}{H_0} \int_0^z \frac{dz'}{(1+z')^{3/2}} \right)^3 \text{ Mpc}^3$$

or $V_C = 8 \times 10^9 \text{ Mpc}^3$ for $z = 0.4$ and $H_0 = 75$. We then expect $(3 \times 10^{-3} \text{ Mpc}^{-3}) \times (8 \times 10^9 \text{ Mpc}^3) \times (4.1 \times 10^{-9}) = 9.8 \times 10^{-2}$ galaxies to be both ULIGs and QSOs by chance. In contrast, we have at least 7 such objects in this volume.

All of this is to say that the presence of both phenomena in one galaxy must necessarily be physically related. By presenting a sample of 8 bona fide QSOs, 7 of which are also bona fide ULIGs, we are firmly establishing the connection between the two phenomena, at least in the objects in our sample. Moreover, the commonly held view that QSOs are fueled in strong tidal interactions has up until now been mostly based on circumstantial evidence. Here we have firmly established that at least some QSOs can be traced back to a merger and an ultraluminous infrared phase.

5.3. Far Infrared Colors

One of the initial goals of this project was to put the transition objects on an age sequence. In an evolutionary scenario where objects move slowly across the FIR diagram, we would have expected those objects with younger ages to be closer to the ULIG region, and those with older ages closer to the QSO region.

In Figs. 10a and b we compare starburst ages for the objects with their position in the FIR diagram in two different ways. First, in Fig. 10a we plot the ratio of the *IRAS* flux density at $25 \mu\text{m}$ to that at $60 \mu\text{m}$, $f(25)/f(60)$, for each object, against its corresponding starburst age. The ratio $f(25)/f(60)$ has been commonly used to isolate candidate objects in searches for active galactic nuclei. Low et al. (1988) note that while the flux at $60 \mu\text{m}$ is in many cases strongly affected by cool emission from star-forming regions outside the active nucleus, the flux at $25 \mu\text{m}$ “can be even more strongly influenced by activity in the nucleus and serves as an indicator of either warm dust heated by an intense radiation field or nonthermal emission.” The second parameter we use (Fig. 10b) includes both color indices, and has the form $\rho_{\text{BB}} \propto y - bx + c$, where y and x are the indices $\alpha(60, 25)$ and $\alpha(100, 60)$, respectively. The constants b and c are chosen in such a way that ρ_{BB} will measure the perpendicular distance to the line that indicates black-body (thermal) radiation in the FIR diagram. (Fig. 1).

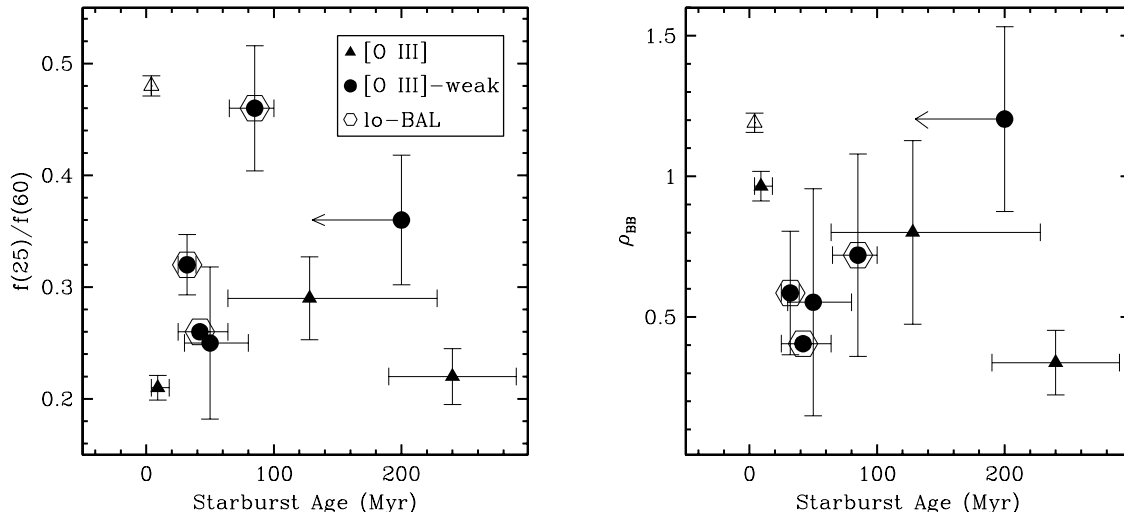


Fig. 10.— FIR Colors vs. starburst ages. The vertical axis on the left plot corresponds to the ratio of *IRAS* flux densities at $25\mu\text{m}$ and $60\mu\text{m}$ while that on the right corresponds to ρ_{BB} , the perpendicular distance from the black body line in Fig. 1. Objects with [O III] emission are plotted as triangles, while those with weak or no [O III] are plotted with circles. I Zw 1 is plotted as an open triangle to indicate the uncertainty in the interpretation of its starburst age (see text) as well as the fact that it has intermediate-strength [O III] emission. Low-ionization BAL QSOs are indicated by hexagons.

It is no surprise that no clear correlation is found in either one of the plots. As discussed above, the transition objects have a rather small range in starburst ages. Considering the uncertainties in age determination, in the precise relation between starburst age and time elapsed since QSO ignition, and in the timescales for buried QSOs to become visible (see below), we do not expect to find a clear correlation between age and FIR colors in our sample even for the case where evolution uniquely determines the FIR colors of the objects.

The fact that the ages for all the transition objects are so young and span such a small range is, however, an important result in itself. The interpretation of this result depends on the relative time scales of the different physical phenomena in these objects. Consider two extreme scenarios:

(1) No evolution in the FIR diagram: The ULIG phase outlives the QSO phase, so that the QSOs in our sample are born in their current position and spend their entire lives there. In this scenario, the small range of starburst ages would indicate that the lifetime of a QSO is very short, *i.e.*, $\lesssim 300$ Myr.

(2) Evolution in the FIR diagram: The QSO phase is longer than the ULIG phase. The QSOs in our sample were born in the ULIG region of the diagram, are now in transition, and will eventually end up in the classical QSO region. In this scenario, our results indicate that the transition stage is very short, *i.e.*, $\lesssim 300$ Myr.

A third possibility, one where objects move from the classical QSO region to the transition region (*i.e.*, galaxies initially hosting QSOs undergo major mergers and become ULIGs as well) has been dismissed in §5.2. In §6 we will discuss whether our results support either one of the two scenarios proposed above, and in §7 we will propose additional observations that can help discriminate between the two of them.

5.4. [O III] Emission

Two points are worth noting regarding [O III] emission in the transition objects. First, there is a high incidence of [O III]-weak objects in our sample (5 out of 9), *i.e.*, objects whose $\text{REW}_{[\text{O III}]} < 5 \text{ \AA}$. [O III]-weak QSOs are uncommon in samples of radio-quiet QSOs (*e.g.*, $\sim 10\%$ in Boroson & Green 1992, or $\sim 20\%$ in Stockton & MacKenty 1987), and even less common in samples of radio-loud quasars (*e.g.*, only 1 out of 45 in Corbin 1997, or 1 out of 58 in Brotherton 1996). Second, there is a known correlation between the presence of strong extended emission and strong nuclear narrow-line emission in QSOs (Boroson & Oke 1984; Stockton & MacKenty 1987). The two transition objects that show strong extended emission, Mrk 1014 and 3C 48, also show the strongest nuclear emission. We will refer back to these two points in the following sections.

5.5. Broad Absorption Line QSOs

BAL QSOs are relatively rare, comprising only about 12% of all radio-quiet QSOs in current magnitude limited samples. The broad, blueshifted troughs in the spectra of BAL QSOs are indicative of high velocity (up to $\sim 0.1 c$) outflows. Although BAL QSOs may form a class independent from non-BAL QSOs, the close similarity in emission lines and continuum properties in these two kinds of objects would seem to indicate that they are physically the same kind of object. Therefore the small fraction of BAL QSOs most likely indicates either a small covering factor of the absorbing material (so that every QSO has a BAL region that covers only about 10% of the solid angle subtended at the effective continuum source), or a short-lived phase in the life of a QSO (see *e.g.*, Weymann 1997 and references therein).

An even rarer class comprising only $\sim 1.5\%$ of all radio-quiet QSOs in optically-selected

samples is that of low-ionization BAL QSOs (hereafter lo-BAL QSOs), which show absorption from low-ionization ionic species such as Mg II, Al III, Si II, and Na I. These objects cannot generally be explained by simple orientation effects since their properties show significant departures from those of non-BAL QSOs: they have stronger emission from Fe II and possibly Fe III, weaker C III], Lyman α , and N V emission lines, and are substantially redder than non-BAL QSOs shortward of 2200 Å (Weymann et al. 1991; Sprayberry & Foltz 1992). Thus lo-BAL QSOs are thought to constitute a different class of radio-quiet QSOs, having more absorbing material and more dust (Voit, Weymann, & Korista 1993; Hutsemékers, Lamy, & Remy 1998).

Six out of the nine objects in our sample have published UV spectra with enough signal to noise to determine whether they are lo-BAL QSOs (Lanzetta, Turnshek, & Sandoval 1993; Turnshek et al. 1997). It is remarkable that three of these objects (IRAS 07598+6508, Mrk 231, and PG 1700+518) are lo-BAL QSOs. Given an intrinsic probability of 0.015, the probability that at least 3 out of the 6 objects with good UV spectra are lo-BAL QSOs by chance is 6.5×10^{-5} . However, considering that the nuclear continuum of lo-BAL QSOs is reddened, their fraction could be significantly underestimated in optically-selected samples. Sprayberry & Foltz (1992) estimate that lo-BAL QSOs may be under-represented in optically selected samples by about an order of magnitude, so that their fraction is more like 0.15. This would also at least partially account for the high incidence of lo-BAL QSOs in warm *IRAS* selected objects previously noticed by Low et al. (1989) and which we also see in our sample. Using this corrected fraction, the a priori probability discussed above raises to 0.05.

We have searched the literature for additional cases of lo-BAL QSOs at low redshift. Sowinski, Schmidt, & Hines (1997) have compiled a catalog that includes nearly every known BAL QSO. From their catalog, as well as the lists of BAL QSOs published by Junkkarinen, Hewitt, & Burbidge (1991) and Barvainis & Lonsdale (1997), we find 19 BAL QSOs with $z < 0.4$ and $\delta > -30$ deg; four of those are confirmed lo-BAL QSOs, including IRAS 07598+6508, PG 1700+518, and Mrk 231. (The recently discovered class of radio-loud BAL quasars does not yet include any objects with $z < 0.4$; M. S. Brotherton, private communication; see also Becker et al. 2000). Therefore, to the best of our knowledge, our sample contains *three of the four confirmed lo-BAL QSOs* that fall in our redshift bin and declination range. The fourth lo-BAL QSO is IRAS 14026+4341 ($z = 0.3233$, $M_B = -24.1$), which shows weaker absorptions similar to those of Mrk 231 (D. C. Hines, private communication). Although not part of our sample, this object appears to be closely related to the objects in our sample. Fig. 1 shows that IRAS 14026+4341 has a position in the FIR diagram fairly close to the (relatively arbitrary) limits of our sample. Its FIR index $\alpha(60, 25)$ is well within the range of our sample, while $\alpha(100, 60)$ is less than 1σ from our limits. In addition, *HST* WFPC2 archival images show that this object has an extended tail and an interacting companion

or large starburst region 2'5 (9.6 kpc) away from the QSO nucleus. Finally, the nuclear spectrum of this object shows no [O III] emission (Turnshek et al. 1997) and strong Fe II emission ($\text{Fe II}/\text{H}\beta \approx 1.0$; Lípari 1994). Thus, it appears that, at least for this small sample of lo-BAL QSOs, all the objects have very similar FIR and optical properties.

Boroson & Meyers (1992) and Turnshek et al. (1997) have noted a correlation between weak nuclear [O III] emission (equivalent widths less than 5 Å) and the presence of low-ionization absorption troughs in QSOs. We have found this tendency in our sample as well. Of the six objects observed in the UV, the three that are lo-BAL QSOs are also [O III]-weak QSOs with $\text{REW}_{[\text{O III}]} \leq 2 \text{ \AA}$, whereas the three objects that are not BAL QSOs have $\text{REW}_{[\text{O III}]} \geq 20 \text{ \AA}$ (see Table 3). We also confirm the previously noticed tendency for these objects to show strong Fe II, which will be discussed further in the following section.

Thus, our observations confirm trends noted before. To these we add the following, for at least the small sample of 4 low-redshift lo-BAL QSOs: (1) they have a small range in FIR colors, (2) all four objects have strong signs of tidal interaction (likely major mergers), (3) at least the three objects in our sample show interaction-induced enhanced star formation, with post-starburst ages $\lesssim 300 \text{ Myr}$.

Our results then support those interpretations of the lo-BAL phenomenon which imply young systems, either in the form of young QSOs “in the act of casting off their cocoons of gas and dust” (Voit, Weymann, & Korista 1993; see also Egami et al. 1996 and Hazard et al. 1984), or as the result of outflows driven by supermassive starbursts (Lípari 1994; Shields 1996). We will return to this point in §6.

It would be of interest to investigate further the possibility that lo-BAL QSOs are exclusively associated with young systems by carrying out spectroscopic and high resolution imaging observations of the host galaxies of larger samples of lo-BAL QSOs. Currently, there are no other studies on the stellar populations of the host galaxies of lo-BAL QSOs. In Canalizo, Stockton, & Roth (1998) we have described a $z \sim 2$ BAL QSO that may be low-ionization (but this needs to be confirmed spectroscopically). The host galaxy shows some asymmetry, and a crude estimation of the age of the stellar populations in the host galaxy from colors yields $\sim 500 \text{ Myr}$. If we can firmly establish that the lo-BAL phenomenon represents a short phase in the early life of QSOs and place limits on the duration of this phase, we could potentially place limits on the mean lifetime of the QSO activity. To this end, it would be necessary to also establish what fraction of QSOs go through a lo-BAL phase, and an accurate, unbiased value for the total fraction of lo-BAL QSOs. As a numerical example, our current results would indicate that the mean lifetime of QSOs is about $300 \text{ Myr} \times (0.15)^{-1} \times (0.5) = 1 \text{ Gyr}$, where 0.15 is the fraction of lo-BAL QSOs (including the correction factor of Sprayberry & Foltz (1992)), and 0.5 is the fraction of the objects in

our sample that undergo a BAL phase (assuming that the homogeneous ages in the sample indicate that the non-lo-BAL QSOs never went through a lo-BAL phase; we will see in §6 that this may not be the case). This is, once again, only an example, as our very small number statistics and the remaining unknowns prevent us from taking this estimate very seriously.

5.6. Fe II Emission

Although the Fe II emission in AGNs has been extensively studied (Joly 1991 and references therein), its origin and nature are still poorly understood. The orthodox view is that the Fe II emission and other low-ionization broad lines (such as Mg II $\lambda 2798$) are produced in high density, high optical-depth regions of broad-line clouds, but current photoionization models do not explain the large Fe II/H β ratios observed in some AGNs.

The nuclear spectrum of every object in our sample shows Fe II emission. With the exception of IRAS 04505–2958, which has a ratio of Fe II $\lambda 4570$ /H β = 0.8, every object is either a strong or extreme emitter according to the definition given in §4. Such high ratios are relatively rare in QSOs, with less than 20% of both radio-loud and radio-quiet QSOs being strong emitters (*e.g.*, Boroson & Green 1992; Joly 1991; Corbin 1997; McIntosh et al. 1999). Only a handful of low-redshift QSOs with extreme Fe II emission are known (Lípari 1994), and two of them (IRAS 07598+6508 and Mrk 231) are part of our sample (Lípari lists I Zw 1 as an extreme emitter as well; however, it is unclear how he obtained such a high Fe II ratio). Therefore, it seems likely that the objects in our sample have a common characteristic which enables the production of strong Fe II emission.

In §2 we described an evolutionary sequence proposed by Lípari (1994) connecting the strength of the Fe II emission with the time elapsed since a major starburst. We find no clear correlation between Fe II $\lambda 4570$ /H β and starburst peak age (Fig. 11). Once again, this is not surprising given the small range and relatively large uncertainties in the ages. While we do not clearly see the trend suggested by Lípari, we do find that the extreme Fe II emitters are among the youngest objects in our sample, and that all of the objects have undergone recent starbursts. Thus, our results could, in principle, fit with Lípari’s and Terlevich et al.’s (1992) suggestion that the Fe II emission arises principally in superwind generated by the starbursts. One problem with this model is, however, that such a wind would presumably have to produce the velocities characteristic of the apparent widths of the Fe II lines, typically 2000–3000 km s^{−1}, considerably higher than well-documented superwinds.

A different trend which is evident in Fig.11 is that [O III] objects (triangles) have weaker

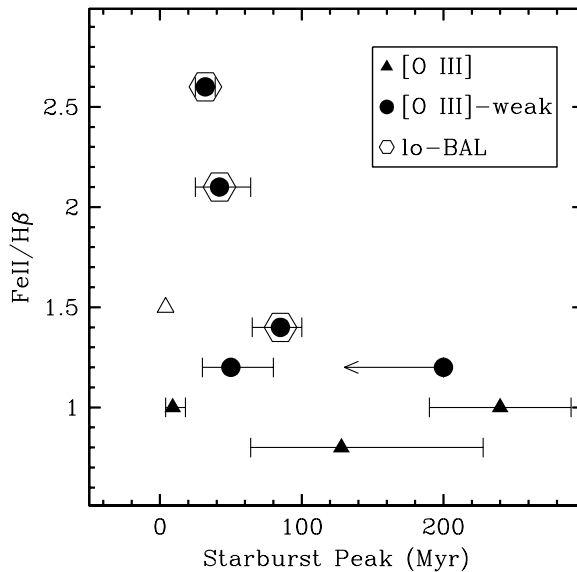


Fig. 11.— Fe II $\lambda 4570/H\beta$ vs. Starburst Age. Symbols are as in Fig. 10.

Fe II emission. This inverse correlation was initially found by Boroson & Green (1992) in low-redshift, radio-quiet QSOs, and it has been confirmed in samples of both radio-loud and radio-quiet QSOs at low, intermediate, and high redshift (*e.g.*, Corbin & Boroson 1996; Brotherton 1996; McIntosh et al. 1999). Of the 15 strong Fe II emitters in Boroson & Green’s sample, 8 have $REW_{[O III]} < 5 \text{ \AA}$, and all 15 of them have $REW_{[O III]} \lesssim 20 \text{ \AA}$ (with IZw 1 being at the top of this range). In our sample, while [O III] objects (except for IZw 1) have the lowest Fe II ratios, these ratios are still higher than the median in QSOs (~ 0.5 ; July 1991), and certainly higher than other QSOs of comparable [O III] emission strength. Thus, the objects in our sample are able to produce strong Fe II emission even when [O III] emission is present.

6. All Things Considered...

The predominant QSO properties observed in the sample, such as strong Fe II, lo-BAL troughs, and weak [O III] emission, all imply a low ionization parameter. Trends indicate also that, at some level, we have two distinct populations: objects with strong [O III] $\lambda\lambda 4959, 5007$ emission, and those with weak or no [O III] emission. There are at least two instances in which QSO spectra can show no [O III] emission: if the upper level of the [O III] lines is collisionally de-excited, or if it is shielded from the strong UV continuum. We now consider

a few reasonable models that might account for the observed properties of the objects in the sample.

(1) The broad absorption line region (BALR) is shielding the UV radiation: Boroson & Meyers (1992) point out that the correlation between very weak [O III] and the presence of lo-BALs strongly suggests that the BALR has a large covering factor (close to 1), preventing much of the ionizing radiation from reaching the low density gas farther away from the QSO nucleus where the [O III] emission is produced. If the BALR has a high physical density as proposed by Boroson & Meyers (1992) and Weymann et al. (1991), then the excess Fe II may arise in the BAL clouds themselves (Sprayberry & Foltz 1992). This model would be consistent with the young ages found in our sample if the lo-BAL phenomenon indeed represents a phase in the early life of QSOs and it would also account for the observed relation between nuclear and extended [O III]. A problem with this model is, however, that there is a large fraction of objects having weak [O III] and strong (or moderately strong) Fe II that do not have BAL spectra, *e.g.*, only 6 out of 18 [O III]-weak objects are BAL QSOs in the study by Turnshek et al. (1997), or only 1 out of 10 in the study by Boroson & Green (1992). If one takes this model to be the only mechanism responsible for producing the rare class of [O III]-weak objects, then these numbers imply a small covering factor for the BALR, and this is at odds with the original premise of this model (*i.e.*, correlation of weak [O III] and BALs). A second problem with this model is that it does not explain the excess Fe II in the strong [O III] emitters in our sample, *i.e.*, those objects where the UV radiation would not be almost completely obscured by the BALR.

(2) Dusty torus model: An obscuring torus of dense, low-ionization gas and possibly dust surrounding the nucleus was first proposed by Weymann et al. (1991) to explain the nature of (both high- and low-ionization) BAL QSOs. BAL clouds are ablated from the surface of the torus and accelerated by thermal wind and radiation pressure, and we view objects as BAL QSOs when the high-velocity outflow lies along the line of sight (*i.e.*, when the torus is seen at high inclination relative to the line of sight); lo-BAL QSOs are then QSOs seen along the most absorbed and dusty lines of sight (Brotherton et al. 1997). This model has been very successful at explaining the polarimetric properties of both classes of BAL QSOs (*e.g.*, Wills et al. 1992; Glenn, Schmidt, & Foltz 1994; Cohen et al. 1995; Hines & Wills 1995), as systems seen near edge-on are expected to be more highly polarized than those seen face-on. Using this model, Wills & Hines (1997) have formed an orientation sequence for a sample of low-redshift FIR-loud objects which includes 7 of the objects in our sample (with only 3C 48 and PG 1543+489 missing from their sample). In this sequence, the highly polarized hyperluminous infrared galaxies are those QSOs where the torus is seen edge on. As the inclination angle decreases, while the polarization is still very high, a reddened QSO becomes visible and the BAL clouds (which are the “skin” of the torus) come

into the line of sight. At even lower inclinations, as the torus is seen nearly face-on, the QSO is unobscured and the amount of polarization drops. Mrk 1014 and IRAS 04505–2958 are included in the latter class, while the other 5 objects in common with our sample are included in the intermediate class (dust torus seen at high inclination). Wills & Hines (1997) note that this sequence could be explained instead by decreasing dust content, but argue that the L_{ir}/L_{opt} of the reddened objects does not appear to be enhanced with respect to that of the PG QSOs when corrected for line-of-sight reddening. The correlation with strong Fe II and weak [O III] emission is not as obvious in this orientation-dependent model. A possibility suggested by D. C. Hines (Hines & Schmidt 1997, comment during question period) is that the Fe II gas may not be physically associated with the torus, but rather lie closer to the central source in dense, matter dominated blobs. While the side of each blob facing the central engine would be highly ionized, the side facing away from it and towards the torus would be less ionized and could give rise to Fe II emission, which could naturally be seen more easily in systems closer to edge-on. In order to explain an orientation dependent [O III], however, anisotropic [O III] emission is required. Hes, Barthel, & Fosbury (1993) argue that, unlike the case of the [O II] $\lambda 3727$ line, the relatively higher ionization potential and critical density of the [O III] $\lambda 5007$ line would allow for a major contribution to its integrated luminosity to come from nuclear regions on a scale not much larger than the broad line region (BLR). Then the [O III] emission could be partially obscured by the dust torus when seen from a range of inclinations. Hes et al. point out that if this were the case, part of the emission may show up weakly in the reflected polarized spectrum, but this has not been observed in any of the polarimetry studies of lo-BAL QSOs (see also Simpson 1998 for an argument against obscured [O III] emission). Even assuming an obscured [O III] emission, the correlation between nuclear and extended emission is not explained, neither is the enhanced Fe II emission in the three objects that are supposedly seen near face on. In addition, the radio properties of lo-BAL QSOs seem to pose a problem to this model. Gregg et al. (2000) argue that no preferred viewing orientation is necessary to observe BAL systems in the spectra of quasars since Gregg et al. and Becker et al. (2000) observe BALs in both flat and steep spectrum quasars, *i.e.*, objects that are presumably viewed along the jet axis and at high inclination respectively (see also Brotherton et al. 1997). Finally, the youth in the transition objects would be fortuitous in this model.

(3) Unusually high densities in the BALR: Weymann et al. (1991) propose an alternate model for lo-BAL QSOs where only the objects falling at the very high end of the column-density distribution of BAL QSOs develop low-ionization absorption and associated Fe II emission. The BALR is taken to be hospitable to dust, which would explain the observed FIR emission and the reddened spectra of these objects. The covering factor is estimated to be 25%–30%. This model then predicts that for every lo-BAL QSO there should be two

or three non-BAL QSOs with comparable IR colors, which is precisely what we see in our sample (assuming the three objects that have not been observed in the UV are not lo-BAL QSOs). While the weak nuclear [O III] is not explicitly accounted for in this model, one might imagine a scenario where the high density in the BAL clouds is able to collisionally de-excite the upper level of [O III]. However, the model does not explain the absence of extended [O III] emission in the majority of the objects in the sample in spite of the fact that all of them are quite likely to have extended gas leftover from the tidal interaction. In addition, there is no clear connection between the model and the youth of the objects in our sample.

(4) Cocoon-like dust surrounds the nuclear regions of the QSO: We have alluded to several lines of evidence supporting the presence of large amounts of dust in the nuclear regions of the transition QSOs (SCC98, CS00a,b, §3). Here we present a model where a dust cocoon is shielding the NLR from the ionizing radiation coming from the central continuum source. The resulting low-ionization parameter and the dusty environment would allow strong Fe II emission to arise, while the absence of extended [O III] emission would be explained by the inability of the ionizing photons to reach the extended gas. The lo-BAL phenomenon would then be interpreted as more widespread outflows, and, as proposed by Voit, Weymann, & Korista (1993), “a manifestation of the [QSO’s] efforts to expel a thick shroud of gas and dust”. In this model, strong [O III] objects are more evolved, having undergone the lo-BAL phase already, and having thus poked some holes through the dusty cocoon. Ionizing photons are then able to reach the NLR through the holes, and also to ionize some of the extended gas. The idea of an ionizing continuum being able to reach the extended gas only along some lines of sight is supported by the patchy morphology of the extended region in 3C 48 and Mrk 1014 (Stockton & MacKenty 1987; CS00a,b) and the fact that much of the gas in their host galaxies is not ionized. This is also consistent with the fact that the three strong [O III] objects are less reddened or obscured than the rest of the objects in the sample. However, even at this stage, much of the dust is still present in nuclear regions (see, *e.g.*, Klaas et al. 1997 and Haas et al. 1998 for dust contents in 3C 48), so that Fe II emission, while less efficiently than in previous stages, is still able to form. The idea of a cocoon with holes may also explain the different lightpaths in BAL QSOs inferred from polarimetric studies, where some continuum is seen to escape without passing through dust (*e.g.*, IRAS 07598+6508: Hines & Wills 1995). A problem with this model is that it is not clear whether a dust cocoon alone would be able to completely suppress the [O III] emission in the majority of the transition objects while at the same time allowing the broad emission lines to be visible, without having to place stringent constraints on allowed dust grain sizes. Other mechanisms which thrive in dusty environments may need to be invoked. For example, Wills & Brotherton (1996) propose an explanation for the strong Fe II–weak

[O III] correlation where a dusty low-ionization BLR (more specifically, dense, high-speed, Fe II-emitting clouds) cover the ionizing continuum, thereby simultaneously increasing the Fe II emission and shielding the lower-density, more distant gas where the [O III] emission is produced. Finally, the youth in 3C 48 implied by its stellar populations pose a problem if 3C 48 is to be considered a more evolved object. It is possible that, being a very powerful object as implied by its very powerful radio source, 3C 48 was able to break through parts of the dust cocoon more rapidly than other objects. This may, in fact, be the reason why lo-BAL QSOs are seemingly more rare among radio-loud sources, and so far only one out of 30+ known radio-loud BAL quasars has been found to have very strong radio emission (Gregg et al. 2000).

While some of these models may be quite appropriate for classical QSOs, the results presented in this paper imply that a model describing transition QSOs must necessarily account for the young ages of these systems. In principle, each of these models could be modified to account for the youth in these systems if, for example, the dusty torus described in (2) was preferentially found in young systems, or the unusually high densities of (3) were a direct result of a violent tidal interaction. For the time being, however, we favor (4) as the working model simply because it accounts for all the observed properties and, in particular, it is a direct consequence of the youth in the systems.

We are now ready to present a cartoon picture of our proposed model: Some major mergers between galaxies of similar mass, often disk galaxies, trigger intense bursts of star formation. As the gas concentrates in nuclear regions, the QSO activity is ignited. Both the starburst and QSO activity start before the galaxies merge if both galaxies lack a substantial bulge, or near the final merger if at least one does have a bulge. Along with gas, dust is concentrated in the central 1 or 2 kpc, resulting in a dust enshrouded QSO. Both the AGN and the starburst heat the dust and the object is observed as a ULIG. A lo-BAL phase comes next when the QSO casts off its cocoon. While we are already able to see the QSO, much of the dust cocoon is still shielding the ionizing UV radiation, so that Fe II is able to survive and oxygen is not doubly ionized in the NLR or extended gas. As the ionizing photons are able to escape along some lines of sight, nuclear and extended [O III] appear. Powerful QSOs, especially powerful radio sources, are able to break through the dust cocoon more rapidly, and this is the reason why we do not see many strong radio-loud quasars in cocoon phase. The entire process does not last very long; transition QSOs either evolve into classical QSOs or die within a few hundred Myr.

In this scenario, our results indicate that we are able to see the radio-quiet QSOs ~ 50 Myr after the peak of the starburst activity. This remarkably short time may appear, at first, to be at odds with the idea that ULIGs evolve to become QSOs, since some ULIGs

have been observed to have starburst ages $\gtrsim 300$ Myr (Surace et al. 1998; Tran et al. 1999²).

However, on the one hand there must be a dispersion in the properties of ULIGs that govern the time it takes for dust to be cleared from the inner regions. On the other hand, as mentioned in CS00a, and in agreement with the scenario proposed above, there is almost certainly a range of lines of sight in each transition object for which the QSO is hidden and the object is viewed solely as a ULIG. In the same way, one might expect that some of the objects that we observe solely as ULIGs are seen as QSOs along some lines of sight. The overlap in ages is then not only consistent, but also expected in the proposed scenario.

One might also expect that some of the latter proposed objects (*i.e.*, hidden QSOs residing in ULIGs) have already poked holes not along our line of sight and are able to ionize the extended gas. Therefore, narrow-band imaging (centered around observed-frame [O III]) of ULIGs may show in some objects extended emission line regions analogous to those of 3C 48 or Mrk 1014 (Canalizo et al., in preparation). Indeed, the ULIG IRAS 09104+4109 ($z = 0.44$, $\log(L_{ir}/L_{\odot}) = 12.65$), which shows a hidden QSO spectrum in polarized, scattered light (Hines et al. 1999a), also shows extended [O III] emission (Armus, Soifer, & Neugebauer 1999; Kleinmann et al. 1988). Tran, Cohen, & Villar-Martin (2000) suggest that the ionized gas is tidal debris, as is likely the case in the two transition objects in our sample with strong extended [O III] (Stockton & MacKenty 1987). Along similar lines, by considering the properties that are common to ULIGs that unambiguously show hidden broad line regions in polarized light, Tran et al. (1999) find that ULIGs are most likely to host an obscured QSO if they exhibit a high-ionization spectrum characteristic of Seyfert 2 galaxies (see also Veilleux, Sanders, & Kim 1997). Incidentally, the newly found “hidden quasar” presented by Tran et al. (1999) (IRAS 17345+1124, $z = 0.162$, $\log(L_{ir}/L_{\odot}) \approx 12$) shows optical Fe II emission.

The eight objects in the sample that are ULIGs have very high IR luminosities, namely $\log(L_{ir}/L_{\odot}) \geq 12.4$. Veilleux, Kim, & Sanders (1999) find that $\sim 50\%$ of ULIGs with $L_{ir} \geq 12.3$ show evidence for nuclear activity, with either Seyfert 1 or Seyfert 2 spectra (the latter presumably being hidden QSOs). This percentage is likely to be even higher at $\log(L_{ir}/L_{\odot}) \geq 12.4$ (D. B. Sanders, private communication). Thus, the objects in the sample may be representative of a large fraction of ULIGs at high luminosities, and our results could, in principle, be consistent with a scenario where a majority of ULIGs at these luminosities go through a transition phase.

²Note, however, that while Tran et al. report finding typical E+A spectra in these galaxies, they do not include an “E” component in modeling the populations. Therefore their ages should be regarded as upper limits when comparing them to the ages we derive.

It is more difficult to estimate what fraction of optically selected QSOs might be represented by our sample. Sanders et al. (1989) show the distribution of the ratio L_{IR}/L_{UV} for PG QSOs (their Fig. 5), having a mean ratio of 0.4 ± 0.15 . If we assume that the ratio $\nu f_{60}/\nu f_B$ for the sample objects listed in column 4 of Table 3 is representative of the ratio given by Sanders et al. and we scale it using Mrk 1014 (which is a member of both the PG sample and our sample), then the transition objects in our sample (excluding Mrk 231, which is not a bona fide QSO and is obviously heavily reddened) have a mean ratio of 1.28 ± 0.95 . By comparing the distributions, we estimate that the transition sample is representative of $\sim 7.5\%$ of the optically selected PG QSO sample. Taking this number at face value would imply that a considerable fraction of optically selected QSOs do not go through a transition phase, unless the QSO activity can last as long as ~ 4 Gyr. However, the ratio of IR to UV luminosities should be treated with caution. While the FIR emission is expected to be emitted isotropically, the flux at UV wavelengths can be significantly depressed with the presence of a screen of dust along the line of sight. Thus this ratio is very likely more indicative of reddening than of intrinsic characteristics in the objects.

Finally, a word on radio-loud vs. radio-quiet QSOs. Our results do not shed any light on possible relationships or differences between the two classes of objects. However, these results give no indication that the two classes form differently. Of nine objects, we have one radio-loud QSO (3C 48), which is exactly how many we would expect in a near-complete sample including both kinds of QSOs. Of the properties we studied in the different objects, all of them were virtually identical in 3C 48 and Mrk 1014: morphologies, starburst timescales, and nuclear properties. The newly discovered class of lo-BAL quasars of moderate radio luminosity (Becker et al. 2000) shows that, in this scenario, radio loud objects can indeed undergo an outflow phase. The fact that strong Fe II emitters are less numerous and [O III]-weak objects are almost non-existent in radio-loud QSOs could be explained as a selection effect: extended radio structure indicates to some level that UV radiation has already been able to escape. This would also explain why Fe II emission appears weaker in lobe-dominant radio-loud QSOs (Wills 1996). Radio-loud QSOs seem to have intrinsically stronger nuclear and extended [O III] emission than radio-quiet QSOs (*e.g.*, Boroson & Oke 1984; Stockton & MacKenty 1987; Wills & Brotherton 1996), and this may in turn be indicative of a more powerful ionizing radiation that can break through obscuring material more rapidly than radio-quiet QSOs. In noticing differences between radio-loud and radio-quiet QSOs, Wills (1996) comments: “The presence of a hot, dusty, environment with low- and high-ionization (BAL) outflows along the line-of-sight [in radio-quiet QSOs] therefore has something to do with *lack* of powerful radio emission”. In our model, the connection would simply be that those systems lacking powerful radio emission take a longer time to get rid of the very dust that is connected with such characteristics.

The model we have presented is by no means complete or unique; most likely there are elements of each of the different models discussed above which play a role in actual systems. Our intention is simply to lay the foundations for a working model that can be tested with observations and, most importantly, that incorporates the new ingredient we have found in these systems, *i.e.*, that they are recently fed AGNs residing in dynamically young systems with young post-starburst populations.

And now for the question of evolution. In §5.3 we stated that the young ages found for the sample objects suggest two possible scenarios: one where objects evolve in the FIR diagram and the transition between groups is fast, and the other where objects do not evolve and the QSO activity is short lived. After analyzing our results as a whole, we find no strong evidence that uniquely supports either one of these scenarios. We may be inclined to favor an evolutionary scenario simply because, based on the model we propose, transition objects could evolve naturally into classical QSOs if only given enough time. However a conclusive answer will only be reached as we gain knowledge on the relative timescales of the two governing phenomena in these systems. In the following section, we describe further observations that may help to settle the question of evolution.

7. Further Tests on the Evolutionary Paradigm

If we could determine the mean lifetimes for the QSO and ULIG phenomena, the question of evolution vs. no evolution in the FIR diagram would be, in principle, unambiguously solved. Unfortunately, there are no simple ways to determine these lifetimes. In §5.5 we proposed a method to estimate the mean lifetime of QSOs from observations of lo-BAL QSOs, but many unknowns need to be solved for before accurate estimates can be obtained, even if the method does turn out to be applicable. For ULIGs, we could possibly observe spectroscopically a large sample and set upper limits to the time a galaxy might spend in this phase. However, the question of whether every ULIG harbors an AGN is far from settled, and this alone could confuse the results.

A different approach to the problem is to try to find the natural descendants of the transition objects, *i.e.*, classical QSOs whose host galaxies contain older starburst populations and aging signs of interaction. We would select a sample of objects with the same selection criteria as the sample in this paper, except that the objects would have a position in the FIR color-color diagram farther away from ULIGs, in the region labeled QSO. These objects are marked by squares in Fig. 1.

The host galaxies of these objects would then be observed with two main objectives: (a)

search for and characterize past interaction or merger activity, and (b) search for and date aging post-starburst populations. The presence of merger remnants (or lack thereof) would certainly establish the role of mergers and interactions in the triggering of the bulk of the QSO population. The presence of aging starburst populations would imply a starburst-AGN connection as in the transition objects. The combination of both results would conclusively establish the connection between classical and transition QSOs, and, therefore, ULIGs. Finally, results would give a measure for the relative time scales of these various phenomena.

7.1. Signs of Past Interactions and Mergers in Classical QSO Host Galaxies

Recent *HST* imaging of QSO host galaxies indicates that at least a large fraction of QSOs, both radio-loud and radio-quiet, reside in elliptical hosts (McLure et al. 1999; Bahcall et al. 1997). If major mergers indeed play a significant role in the origin of the majority of the QSO population, it is possible that these elliptical hosts are rather merger remnants (Toomre & Toomre 1972). If this were the case, one might expect to find fine structure indicative of past interaction and ancient merger events in the host galaxies. This tell-tale structure, which includes ripples, plumes, tails, and boxy isophotes, is commonly seen in nearby ellipticals (*e.g.*, Malin 1979; Malin & Carter 1980; Schweizer & Seitzer 1992; Bender et al. 1989), and indicates that at least some of these early type galaxies were either formed or structurally modified by mergers relatively recently (*e.g.*, Hernquist & Spergel 1992; Barnes 1992; Hernquist & Quinn 1988, 1989; Schmidt & Green 1983; Toomre 1977).

In a study of a large sample of nearby E and S0 galaxies, Schweizer and collaborators (Schweizer & Seitzer 1988, 1992; Schweizer et al. 1990) used a fine structure index, Σ , to characterize past merger activity. The index Σ measures four types of fine structure thought to be caused by mergers, and therefore is sensitive to the dynamical age of the merger, and provides a rough measure of the dynamical youth or rejuvenation of the galaxies. Sansom, Hibbard, & Schweizer (2000) found an anticorrelation between Σ and X-ray excess in early type galaxies, which indicates that galaxies with high fine-structure content have not had enough time after the merger to form hot halos.

Ground-based imaging observations using adaptive optics (AO) and space-based imaging observations using the *HST* highly sensitive Advanced Camera for Surveys (ACS) would make it possible to detect such fine structure in the hosts of QSOs. The $\sim 0''.1$ resolution of such observations is equivalent to 0.4 kpc for objects at $z = 0.4$, even better than the 0.5 kpc resolution in Schweizer & Seitzer’s study of nearby galaxies. Thus, it is quite possible to apply these techniques to QSO host galaxies and characterize past interaction and merger activity in these systems.

7.2. Aging Starbursts in Classical QSO Host Galaxies

As we have seen, spectroscopic observations allow us to date directly the ages of the stellar populations in the host galaxies of QSOs. We can use similar techniques to the ones described in this paper to observe and model the host galaxies of classical QSOs.

In order to test the feasibility of detecting older starbursts in host galaxies, we have carried out simulations of different intermediate-age starburst populations superposed on the spectrum of an old elliptical galaxy. The simulations show that it is possible to detect and identify a starburst population as old as ~ 1.3 Gyr that comprises 10% of the total luminous mass along the line of sight. The best age indicators are the Balmer lines ($H\beta$ and $H\delta$ in particular), the 4000 Å break, the CN-band, and, for higher- z objects, the slope of the continuum shortwards of 3100 Å. The flux of starburst populations older than ~ 1.6 Gyr drops very rapidly with age and it becomes difficult to distinguish between a starburst+elliptical spectrum and the elliptical spectrum itself, unless the mass fraction of the starburst population along the line of sight is significantly higher than 10%.

These constraints give us much room to find the descendants of transition objects. As we have seen, our results imply that objects move rapidly from the ULIG to classical QSO population in the evolutionary scenario. Therefore we expect to find descendants (if any) with post-starbursts ages ranging from $\gtrsim 300$ Myr to the upper limit of the QSO lifetime. Dating such relatively young starbursts should be quite feasible.

7.3. An Example: PHL 909

As a preview to what we might expect from these observations, we briefly discuss results for one member of the classical QSO population, PHL 909 ($z = 0.171$), for which analogous observations already exist. The position of PHL 909 in the FIR diagram is indicated in Fig. 1 by a filled square surrounded by a large open square. Fig. 2 of Bahcall et al. (1997) shows a PSF subtracted, *HST* WFPC2 image of PHL 909 through the F606W filter. Bahcall et al. report that the host is a normal E4 galaxy. McLure et al. (1999) successfully model the host with an elliptical template in a F675W *HST* image, which presumably avoids strong emission lines. The QSO+elliptical-host subtracted image shown in their Fig. A11 has structure in the residuals which, pending careful analysis, may be interpreted as the tell-tale structure described in §7.1. A 900 s Keck LRIS spectrum of the host galaxy of PHL 909 (Canalizo & Stockton, in preparation) shows that there is no very young post-starburst component present. However, this spectrum does not have sufficient S/N to constrain the presence of a significant ~ 1 -Gyr-old population.

8. Summary and Conclusions

We have studied a sample of transition QSOs, *i.e.*, bona fide QSOs that have far infrared colors intermediate between ULIGs and QSOs. In summary,

1. Every transition QSO shows signs of tidal interaction. Five out of nine are confirmed major mergers and are in the late stages when the nuclei have already merged. Three additional objects have strongly interacting companions with masses comparable to those of the hosts, and are expected to merge soon (resulting in major mergers as well). Only one transition QSO is undergoing a minor merger.

2. Disk galaxies are often involved in these mergers. Seven objects show clear tidal tails, and one shows a bridge connecting the companion galaxy with the host. Of the objects that have not yet merged, two are likely to be ring galaxies (with tidal tails as well) resulting from near head-on collisions.

3. Every transition QSO shows strong recent star-forming activity, and in eight cases this activity is closely related to the tidal interaction. These eight objects have spectra characteristic of E+A galaxies. The spectra are successfully modeled by an underlying old population plus a superposed young instantaneous burst population. We find very young starburst ages for all the objects in our sample, ranging from ongoing star formation to ~ 300 Myr.

4. By comparing the starburst ages of the central stellar components with those of the more extended emission, we have determined the relative ages between stellar populations in various regions of the host galaxies. These estimates, along with dynamical ages, place constraints on the timescale for concentrating material in the nucleus, which in turn could provide the fuel for the QSO. This is an important step towards understanding the fueling of QSOs, and the timescales for their evolution.

5. Interaction and star-forming activity histories indicate that the age of the QSO activity is more closely correlated with the age of the peak starburst than to the dynamical age of the system.

6. Seven out of the eight bona fide QSOs in the sample are also bona fide ULIGs. The probability that both phenomena coexist by chance in any given otherwise normal galaxy if the two are unrelated is 4.1×10^{-9} . The expected number of galaxies that show both phenomena by chance in the integrated comoving volume spanned by our sample is ~ 0.1 galaxies. Our sample firmly establishes the physical connection between the two phenomena in at least one subclass of QSOs.

7. The young ages derived for the transition QSOs imply one of two scenarios: (a) At

least some ULIGs evolve to become classical QSOs, and the transition time between the two is short ($\lesssim 300$ Myr), or (b) At least some QSOs are born under the same conditions as ULIGs and their lifetime as QSOs is very short ($\lesssim 300$ Myr).

8. We find a high incidence of lo-BAL QSOs, [O III]-weak QSOs, and QSOs with strong or extreme Fe II emission in our sample. We confirm previously reported trends in these properties, and our results require that they be interpreted in the context of young systems.

9. Three out of the four known lo-BAL QSOs with $z \leq 0.4$ and $\delta \geq -30$ deg are part of the sample of transition QSOs. The fourth object has very similar FIR colors, a clear tail, and possibly luminous regions of recent star formation. This indicates that the lo-BAL phenomenon is directly related to young systems, and it may represent a short-lived stage in the early life of a large fraction of QSOs.

10. We find evidence indicating that objects with strong [O III] emission and those with weak or no [O III] represent two distinct populations. The former may be at a more evolved stage in an evolutionary scenario.

11. We propose a model involving a dust cocoon that initially surrounds the QSO nuclear regions, which can account for all the observed and derived properties in transition objects. This model is at least qualitatively consistent with the idea of young, dust-enshrouded QSOs originally proposed by Sanders et al. (1988)

At the beginning of this paper, we posed two important questions regarding the transition objects: “*Where did they come from?*”, and “*Where will they go?*” We have answered the first question unambiguously: transition objects are the product of mergers resulting in vigorous star formation and the ignition of QSO activity. Transition objects have come from, and are still part of, the ULIG population. We have also narrowed down the answer to the second question to two possibilities: either transition objects will indeed go on to become part of the classical QSO population within a few hundred million years, or they will die within this same amount of time. In addition, we have outlined observations that can potentially discriminate between the two possibilities. The final answer to this question will also provide crucial answers regarding the timescales involved in the ULIGs and QSOs.

We thank Gerbs Bauer, Barry Rothberg, and Scott Dahm for assisting in some of the imaging observations. We thank Dean Hines and Mike Brotherton for providing information about BAL QSOs prior to publication, and Dave Sanders, John Tonry, and Esther Hu for helpful discussions. We are grateful to the referee, Sylvain Veilleux, for his careful reading of the paper and useful comments and suggestions. This research has made use of the NASA/IPAC Extragalactic Database (NED) which is operated by the Jet Propulsion

Laboratory, California Institute of Technology, under contract with the National Aeronautics and Space Administration. This research was partially supported by NSF under grant AST 95-29078. Part of this work was performed under the auspices of the U.S. Department of Energy by the University of California Lawrence Livermore National Laboratory under contract No. W-7405-ENG-48.

REFERENCES

- Allen, D. A., Roche, P. F., & Norris, R. P. 1985, MNRAS, 213, 67
- Armus, L., Heckman, T., & Miley, G. 1987, AJ, 94, 831
- Armus, L., Soifer, B. T., & Neugebauer, G. 1999, Ap&SS, 266, 113
- Bahcall, J. N., Kirhakos, S., Saxe, D. H., & Schneider, D. P. 1997, ApJ, 479, 642
- Bahcall, J. N., Kirhakos, S., & Schneider, D. P. 1995, ApJ, 450, 486
- Balick, B. & Heckman, T. M. 1983, ApJ, 265, 1
- Barnes, J. E. 1992, ApJ, 393, 984
- Barvainis, R., Alloin, D., & Antonucci, R. 1989, ApJ, 337, L69
- Barvainis, R. & Lonsdale, C. 1997, AJ, 113, 144
- Becker, R. H., White, R. L., Gregg, M. D., Brotherton, M. S., Laurent-Meuleisen, S. A., & Arav, N. 2000, ApJ, 538, 72
- Bender, R., Surma, P., Dobereiner, S., Mollenhoff, C., & Madejsky, R. 1989, A&A, 217, 35
- Boroson, T. A., & Green, R. F. 1992, ApJS, 80, 109
- Boroson, T. A., & Meyers, K. A. 1992, ApJ, 397, 442
- Boroson, T. A., & Oke, J. B. 1982, Nature, 296, 397
- Boroson, T. A., & Oke, J. B. 1984, ApJ, 281, 535
- Boroson, T. A. & Oke, J. B. 1987, PASP, 99, 809
- Boroson, T. A., Oke, J. B., & Green, R. F. 1982, ApJ, 263, 32
- Boroson, T. A., Persson, S. E., & Oke, J. B. 1985, ApJ, 293, 120

- Bothun, G. D., Romanishin, W., Strom, S. E., & Strom, K. M. 1984, *AJ*, 89, 1300
- Boyce, P. J., Disney, M. J., Blades, J. C., Boksenberg, A., Crane, P., Deharveng, J. M., Macchetto, F. D., Mackay, C. D., & Sparks, W. B. 1996, *ApJ*, 473, 760
- Boyce, P. J., Disney, M. J., Blades, J. C., Boksenberg, A., Crane, P., Deharveng, J. M., Macchetto, F. D., Mackay, C. D., & Sparks, W. B. 1998, *MNRAS*, 298, 121
- Bransford, M. A., Appleton, P. N., Marston, A. P., & Charmandaris, V. 1998, *AJ*, 116, 2757
- Brotherton, M. S. 1996, *ApJS*, 102, 1
- Brotherton, M. S., Tran, H. D., Hien, D., van Breugel, W., Dey, A., & Antonucci, R. 1997 *ApJ*, 487, L113
- Bruzual A., G. & Charlot, S. 1996, unpublished [<ftp://gemini.tuc.noao.edu/pub/charlot/bc96>]
- Canalizo, G., & Stockton, A. 1997, *ApJ*, 480, L5 (CS97)
- Canalizo, G., & Stockton, A. 2000a, *ApJ*, 528, 201 (CS00a)
- Canalizo, G., & Stockton, A. 2000b, *AJ*, 120, 1750 (CS00b)
- Canalizo, G., Stockton, A., & Roth, K. C. 1998, *AJ*, 115, 890
- Cardelli, J. A., Clayton, G. C., & Mathis, J. S. 1989, *ApJ*, 345, 245
- Carone, T. E. et al. 1996, *ApJ*, 471, 737
- Carroll, S. M., Press, W. H., & Turner, E. L. 1992, *ARA&A*, 30, 499
- Clements, D. L., Sutherland, W. J., Saunders, W., Efstathiou, G. P., McMahon, R. G., Maddox, S., Lawrence, A., & Rowan-Robinson, M. 1996a, *MNRAS*, 279, 459
- Clements, D. L., Sutherland, W. J., McMahon, R. G., & Saunders, W. 1996b, *MNRAS*, 279, 477
- Clements, D. L. 2000, *MNRAS*, 311, 833
- Cohen, M. H. et al. 1995, *ApJ*, 448, L77
- Corbin, M. R. 1997, *ApJS*, 113, 245
- Corbin, M. R., & Boroson, T. A. 1996, *ApJS*, 107, 69
- de Grijp, M. H. K., Miley, G. K., & Lub, J. 1987, *A&AS*, 1987, 70, 95

- Disney, M. J., et al. 1995, *Nature*, 376, 150
- Egami, E., Iwamuro, F., Maihara, T., Oya, S., Cowie, L. L. 1996, *AJ*, 112, 73
- Gehren, T., Fried, J., Wehinger, P. A., & Wyckoff, S. 1984, *ApJ*, 278, 11
- Genzel, R. et al. 1998, *ApJ*, 498, 579
- Glenn, J., Schmidt, G. D., & Foltz, C. B. 1994, *ApJ*, 434, L47
- Goodrich, R. W. & Miller, J. S. 1994, *ApJ*, 434, 82
- Goodrich, R. W., Miller, J. S., Martel, A., Cohen, M. H., Tran, H. D., Ogle, P. M., & Vermeulen, R. C. 1996, *ApJ*, 456, L9
- Grazian, A., Cristiani, S., D’Odorico, V., Omizzolo, A., & Pizzella, A. 2000, *AJ*, 119, 2540
- Gregg, M. D., Becker, R. H., Brotherton, M. S., Laurent-Meuleisen, S. A., Lacy, M., White, R. L. 2000, *ApJ*, 544, 142
- Gunn, J. E. 1979 in *Active Galactic Nuclei*, ed. C. Hazard and S. Mitton (New York: Cambridge University Press), p. 213
- Haas, M., Chini, R., Meisenheimer, K., Stickel, M., Lemke, D., Klaas, U., & Kreysa, E. 1998, *ApJ*, 503, L109
- Hazard, C., Morton, D. C., Terlevich, R., & McMahon, R. 1984, *ApJ*, 282, 33
- Heckman, T. M., Bothun, G. D., Balick, B., Smith, E. P. 1984, *AJ*, 89, 958
- Hernquist, L., & Quinn, P. J. 1988, *ApJ*, 331, 682
- Hernquist, L., & Quinn, P. J. 1989, *ApJ*, 342, 1
- Hernquist, L., & Spiegel, D. N. 1992, *ApJ*, 399, 117
- Hes, R., Barthel, P. D., & Fosbury, R. A. E. 1993, *Nature*, 362, 326
- Hickson, P. & Hutchings, J. B. 1987, *ApJ*, 312, 518
- Hines, D. C., Low, F. J., Thompson, R. J., Weymann, R. J., & Storrie-Lombardi, L. 1999, *ApJ*, 512, 140
- Hines, D. C., & Schmidt, G. D. 1997, in *Mass Ejection from Active Galactic Nuclei*, ASP Conference Series 128, ed. N. Arav, I. Shlosman, & R. J. Weymann, p. 99

- Hines, D. C., Schmidt, G. D., Smith, P. S., Cutri, R. M., Low, F. J. 1995, ApJ, 450, L1
- Hines, D. C., Schmidt, G. D., Wills, B. J., Smith, P. S., & Sowinski, L. G. 1999, ApJ, 512, 145
- Hines, D. C., & Wills, B. J. 1995, ApJ, 448, L69
- Hodapp, K.-W., et al. 1996, New Astronomy, 1, 177
- Houck, J. R. et al. 1984, ApJ, 278, L63
- Hughes, D. H., Kukula, M. J., Dunlop, J. S., Boroson, T. 2000, MNRAS, 316, 204
- Hutchings, J. B., Campbell, B., Gower, A. C., Crampton, D., & Morris, S. C. 1982a, ApJ, 262, 48
- Hutchings, J. B., & Crampton, D. 1990, AJ, 99, 37
- Hutchings, J. B., Crampton, D., Campbell, B., Duncan, D., & Glendenning, B. 1984, ApJS, 55, 319
- Hutchings, J. B., Crampton, D., Campbell, B., Pritchett, C. 1981, ApJ, 247, 743
- Hutchings, J. B., Holtzman, J., Sparks, W. B., Morris, S. C., Hanisch, R. J., & Mo, J. 1994, ApJ, 429, L1
- Hutchings, J. B., Johnson, I., & Pyke, R. 1988, ApJS, 66, 361
- Hutchings, J. B. & Neff, S. G. 1988, AJ, 96, 1575
- Hutchings, J. B., & Neff, S. G. 1992, AJ, 104, 1
- Hutsemékers, D., Lamy, H., & Remy, M. 1998, A&A, 340, 371
- Joly, M. 1991, A&A, 242, 49
- Joseph, R. D. 1999, Ap&SS, the Ringberg Workshop, “Ultraluminous Galaxies: Monsters or Babies” (Ringberg Castle, September 1998), 266, p. 321
- Junkkarinen, V., Hewitt, A., & Burbidge, G. 1991, ApJS, 77, 203
- Kim, K.-C. & Sanders, D. B. 1998, ApJS, 119, 41
- Klaas, U., Haas, M., Heinrichsen, I., & Schutz, B. 1997, A&A, 325, L21

- Kleinmann, S. G., Hamilton, D., Keel, W. C., Wynn-Williams, C. G., Eales, S. A., Becklin, E. E., & Kuntz, K. D. 1988, ApJ, 328, 161
- Lanzetta, K. M., Turnshek, D. A., & Sandoval, J. 1993, ApJS, 84, 109
- Lim, J. & Ho, P. 1999, ApJ, 510, L7
- Lípari, S. 1994 ApJ, 436, 102
- Lonsdale, C. J., Smith, H. E., & Lonsdale, C. J. 1995, ApJ, 438, 632
- Lonsdale, C. J., Smith, H. E., & Lonsdale, C. J. 1993, ApJ, 405, L9
- Low, F. J., Cutri, R. M., Kleinmann, S. G., & Huchra, J. P. 1989, ApJ, 340, L1
- Low, F. J., Huchra, J. P., Kleinmann, S. G., Cutri, R. M. 1988, ApJ, 327, L41
- Lutz, D., Spoon, H. W. W., Rigopoulou, D., Moorwood, A. F. M., Genzel, R. 1998, ApJ, 505, L103
- Lutz, D., Veilleux, S., & Genzel, R. 1999, ApJ, 517, L13
- Lynden-Bell, D. 1969, Nature, 223, 690
- Lynds, R., & Toomre, A. 1976, ApJ, 209, 382
- MacKenty, J. W., & Stockton, A. N. 1984, ApJ, 283, 64
- Malin, D. F. 1979, Nature, 277, 279
- Malin, D. F., & Carter, D. 1980, Nature, 285, 643
- McIntosh, D. H., Rieke, M. J., Rix, H.-W., Foltz, C. B., & Weymann, R. J. 1999, ApJ, 514, 40
- McLeod, K. K., & Rieke, G. H. 1994, ApJ, 431, 137
- McLure, R. J., Kukula, M. J., Dunlop, J. S., Baum, S. A., O’Dea, C. P., & Hughes, D. H. 1999, MNRAS, 308, 377
- Meylan, G. 1993, in *The Globular Cluster Galaxy Connection*, ed. G. H. Smith & J. P. Brodie, ASP Conference Series, vol.48, p. 588
- Mihos, J. C. & Hernquist, L. 1994, 425, L13
- Mihos, J. C. & Hernquist, L. 1996, ApJ, 464, 641

- Nakagawa, T., Kii, T., Fujimoto, R., Miyazaki, T., Inoue, H., Ogasaka, Y., Kawabe, R. 1999, *Ap&SS*, 266, 43
- Neugebauer, G., Soifer, B. T., & Miley, G. K. 1985, *ApJ*, 295, L27
- Neugebauer, G., Miley, G. K., Soifer, B. T., & Clegg, P. E. 1986, *ApJ*, 308, 815
- Nolan, L. A., Dunlop, J. S., Kukula, M. J., Hughes, D. H., Boroson, T., & Jimenez, R. 2000, *MNRAS*, in press [astro-ph/0004325]
- Oke, J. B., et al. 1995, *PASP*, 107, 375
- Sanders, D. B. 1999, *Ap&SS*, the Ringberg Workshop, “Ultraluminous Galaxies: Monsters or Babies” (Ringberg Castle, September 1998), 266, p. 331
- Sanders, D. B. & Mirabel, I. F. 1996, *ARA&A*, 34, 749
- Sanders, D. B., Phinney, E. S., Neugebauer, G., Soifer, B. T., & Matthews, K. 1989, *ApJ*, 347, 29
- Sanders, D. B., Scoville, N. Z., Young, J. S., Soifer, B. T., Schloerb, F. P., Rice, W. L., & Danielson, G. E. 1986, *ApJ*, 305, 45
- Sanders, D. B., Soifer, B. T., Elias, J. H., Madore, B. F., Matthews, K., Neugebauer, G., & Scoville, N. Z. 1988, *ApJ*, 325, 74
- Sansom, A. E., Hibbard, J. E., Schweizer, F. 2000, *AJ*, 120, 1946
- Sargent, W. L. W. 1968, *ApJ*, 151, L31
- Scalo, J. M. 1986, *Fund. Cosmic Phys.*, 11, 1
- Schinnerer, E., Eckart, A., & Tacconi, L. J. 1998, *ApJ*, 500, 147
- Schlegel, D. J., Finkbeiner D. P., & Davis, M. 1998, *ApJ*, 500, 525
- Schmidt, M., & Green, R. F. 1983, *ApJ*, 269, 352
- Schweizer, F., & Seitzer, P. 1988, *ApJ*, 328, 88
- Schweizer, F., & Seitzer, P. 1992, *AJ*, 104, 1039
- Schweizer, F., Seitzer, P., Faber, S. M., Burstein, D., Dalle Ore, C. M., & Gonzalez, J. J. 1990, *ApJ*, 364, L33

- Shields, G. A. 1996, ApJ, 461, L9
- Simpson, C. 1998, MNRAS, 297, L39
- Smith, H., E., Lonsdale, C. J., Lonsdale, C. J. 1998, ApJ, 492, 137
- Soifer, B. T. et al. 1984a, ApJ, 278, L71
- Soifer, B. T., Neugebauer, G., Helou, G., Lonsdale, C. J., Hacking, P., Rice, W., Houck, J. R., Low, F. J., & Rowan-Robinson, M. 1984b, ApJ, 283, L1
- Soifer, B. T., Sanders, D. B., Neugebauer, G., Danielson, G. E., Lonsdale, C. J., Madore, B. F., Persson, S. E. 1986, ApJ, 303, L41
- Soifer, B. T., Sanders, D. B., Madore, B. F., Neugebauer, G., Danielson, G. E., Elias, J. H., Lonsdale, C. J., Rice, W. L. 1987, ApJ, 320, 238.
- Sowinski, L. G., Schmidt, G. D., & Hines, D. C. 1997, in *Mass Ejection from Active Galactic Nuclei*, ASP Conference Series 128, ed. N. Arav, I. Shlosman, & R. J. Weymann, p. 305
- Sprayberry, D. & Foltz, C. B. 1992, ApJ, 390, 39
- Stockton, A. 1982, ApJ, 257, 33
- Stockton, A. 1990, in *Dynamics and Interactions of Galaxies*, ed. R. Wielen, (Springer-Verlag: Berlin), 440
- Stockton, A., Canalizo, G., & Close, L. 1998, ApJ, 500, L121 [SCC98]
- Stockton, A., & MacKenty 1987, ApJ, 316, 584
- Stockton, A., & Ridgway, S. E. 1991, AJ, 102, 488
- Surace, J. A., 1998, Ph.D. thesis, University of Hawaii
- Surace, J. & Sanders, D. B. 2000, AJ, 120, 604
- Surace, J. A., Sanders, D. B., Vacca, W. D., Veilleux, S., & Mazzarella, J. M. 1998, ApJ, 492, 116
- Taniguchi, T., Kawara, K., Nishida, M., Tamura, S., Nishida, M. T. 1988, ApJ, 95, 1378
- Terlevich, R., Tenorio-Tagle, G., Franco, J., & Melnick, J 1992, MNRAS, 255, 713

- Toomre, A. 1977, in *The Evolution of Galaxies and of Stellar Populations*, eds. B. M. Tinsley & R. B. Larson (Yale Observatory, New Haven), p. 401
- Toomre, A., & Toomre, J. 1972, *ApJ*, 178, 623
- Tran, H. D., Brotherton, M. S., Stanford, S. A., van Breugel, W., Dey, A., Stern, D., & Antonucci, R. 1999, *ApJ*, 516, 85
- Tran, H. D., Cohen, M. H., & Villar-Martin, M. 2000, *AJ*, in press [astro-ph/0004383]
- Turnshek, D. A., Monier, E. M., Sirola, C. J., & Espey, B. R. 1997, *ApJ*, 476, 40
- Vader, J. P., Da Costa, G. S., Frogel, J. A., Heisler, C. A., Simon, M. 1987, *AJ*, 94, 847
- Vader, J. P., & Simon, M. 1987, *Nature*, 327, 304
- Veilleux, S. 1999, in *Galaxy Interactions at Low and High Redshift (IAU Symp. 186)*, ed. J. E. Barnes & D. B. Sanders (Dordrecht: Kluwer), p. 295
- Veilleux, S. & Osterbrock, D. E. 1987, *ApJS*, 63, 295
- Veilleux, S., Sanders, D. B., & Kim, D.-C. 1997, *ApJ*, 484, 92
- Veilleux, S., Kim, D.-C., & Sanders, D. B. 1999, *ApJ*, 522, 113
- Véron-Cetty, M.P. & Véron, P. 1996, *ESO Sci. Rep.* 17, 1
- Voit, G. M., Weymann, R. J., & Korista, K. T. 1993, *ApJ*, 413, 95
- Weymann, R. 1997, in *Mass Ejection from Active Galactic Nuclei*, ASP Conference Series 128, ed. N. Arav, I. Shlosman, & R. J. Weymann, p. 3
- Weymann, R. J., Morris, S.L., Foltz, C.B., & Hewett, P.C. 1991, *ApJ*, 373, 23
- Wills, B. J. 1996, in *Jets from Stars to Active Galactic Nuclei*, ed. W. Kundt (Berlin: Springer), 213
- Wills, B. J., & Brotherton, M. S. 1996, in *Jets from Stars to Active Galactic Nuclei*, ed. W. Kundt, (Berlin: Springer), p. 203
- Wills, B. J., & Hines, D. C. 1997, in *Mass Ejection from Active Galactic Nuclei*, ASP Conference Series 128, ed. N. Arav, I. Shlosman, & R. J. Weymann, p. 99
- Wills, B. J., Wills, D., Evans, N. J., II, Natta, A, Thompson, K. L., Breger, M., & Sitko, M. L. 1992, *ApJ*, 400, 96

Wyckoff, S., Gehren, T., & Wehinger, P. A. 1981, ApJ, 247, 750

Zheng, Z., et al. 1999, A&A, 349, 735

This figure "f2.jpg" is available in "jpg" format from:

<http://arxiv.org/ps/astro-ph/0103332v1>

This figure "f4.jpg" is available in "jpg" format from:

<http://arxiv.org/ps/astro-ph/0103332v1>

This figure "f6.jpg" is available in "jpg" format from:

<http://arxiv.org/ps/astro-ph/0103332v1>

This figure "f8.jpg" is available in "jpg" format from:

<http://arxiv.org/ps/astro-ph/0103332v1>